Emended Sandbian (Ordovician) conodont biostratigraphy in Baltoscandia and a new species of *Amorphognathus*

Tõnn Paiste[1] , Peep Männik[2] and Tõnu Meidla[1]

[1]Institute of Geology, University of Tartu, Ravila 14A, Tartu 50114, Estonia and [2]Institute of Geology, Tallinn University of Technology, Ehitajate tee 5, Tallinn 19086, Estonia

Abstract

Conodonts are an important biostratigraphic tool for many Phanerozoic stages. Along with graptolites, they define all global Ordovician Stage boundaries. Within the Upper Ordovician interval, a known species of *Amorphognathus tvaerensis* (Bergström) is present in both Sandbian and Katian stratotype sections. Study of changes in the succession of *A. tvaerensis* revealed that elements in the upper part of its range differ morphologically quite distinctly from those in its lower part. Here, they are described as a new conodont species, *A. viirae* sp. nov. This new species is recognized in several Estonian and Swedish sections, with apparent occurrence also in Mójcza Quarry, Holy Cross Mountains, Poland and Black Knob Ridge, Oklahoma, USA. Detailed analysis of early *Amorphognathus* elements from Estonian and Swedish sections revealed the absence of *A. inaequalis* (Rhodes) in both regions, although a conodont subzone based on this species was identified earlier by some authors. Both the absence of *A. inaequalis* (Rhodes) and recognition of the new species *A. viirae* sp. nov. resulted in the revision of the conodont zonation, and a new version of it is proposed for the Sandbian Stage in the Atlantic Realm. The new zonation includes (from below) *Pygodus anserinus*, *Baltoniodus variabilis*, *A. tvaerensis*, *B. gerdae*, *A. viirae* and *B. alobatus* Conodont zones.

CAMBRIDGE
UNIVERSITY PRESS

1. Introduction

Originally, the genus *Amorphogathus* was defined as a formal taxon (Branson & Mehl, 1933) based on an element which was later recognized as Pa of the *Amorphognathus* apparatus. Identification of other elements of the apparatus revealed that the M element can also be used as a diagnostic for different species of the genus *Amorphognathus* (Bergström, 1971). The structure of the apparatus and phylogeny of *Amorphognathus* has been discussed in several papers (Bergström, 1983; Dzik, 1999a; Bergström & Leslie, 2010; Ferretti *et al.* 2014a). It is commonly accepted that S elements of the *Amorphognathus* apparatus are the most conservative; they hardly change during evolution of the genus and are of limited assistance in the identification of the species (Ferretti *et al.* 2014a).

As a rapidly evolving genus with nearly global distribution, *Amorphognathus* is especially useful for stratigraphic purposes (Bergström & Ferretti, 2017); further complementary research on the topic is therefore essential. Among the different species of genus *Amorphognathus*, *Amorphognathus tvaerensis* (Bergström, 1962) has stratigraphic importance in Baltoscandia and Argentine Precordillera (Albanesi & Ortega, 2016). Additionally, *A. tvaerensis* is present in stratotype sections of both the Sandbian (Baltoscandia, Sweden, Fågelsång; Bergström *et al.* 2000) and the Katian (Laurentia, Oklahoma, Black Knob Ridge; Goldman *et al.* 2007) stages, making it a useful species for global correlation. Occurrences of *A. tvaerensis* in the sections of Poland and Scotland are also known (Bergström, 1962). Several authors have discussed variations in elements of *A. tvaerensis* (Dzik, 1990, 1994; Viira, 2008; Xu *et al.* 2010; Paiste *et al.* 2022) but have not drawn any conclusions, probably because of a lack of representative material for such a study. In the present study, which is based on a rich collection of conodonts from the Mehikoorma drillcore section from Estonia, the morphological variation of the P and M elements of the species of genus *Amorphognathus* in the Sandbian and lower Katian interval is analysed in detail, with the aim of clarifying species variation and the resulting implications to stratigraphy.

2. Geological setting

During Sandbian and early Katian (Late Ordovician) time, the Baltoscandian Ordovician Palaeobasin on the western Baltica palaeocontinent was situated close to the tropical realm (Cocks & Torsvik, 2005). The basin is commonly divided into three distinct facies belts,
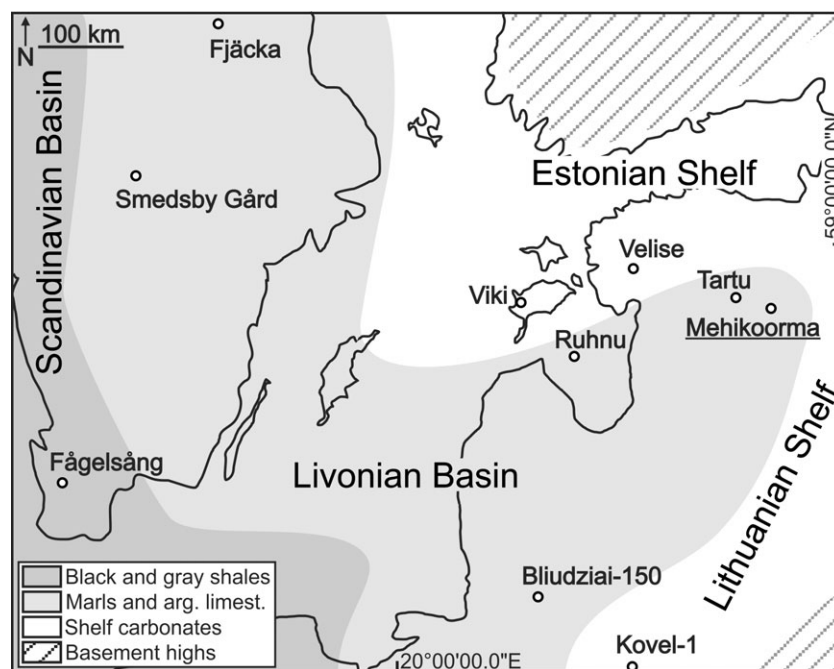
Fig. 1. General facies structure of the Baltoscandian Ordovician Palaeobasin. Locations of the sections discussed or referred to in the text are marked with circles (modified after Männik *et al.* 2021; Paiste *et al.* 2022).

sometimes called also basins (Fig. 1). Western Sweden and northwestern Poland comprise the Scandinavian Basin with graptolitiferous black shales and grey shales. Eastern Sweden, northeastern Poland, the western part of Latvia and Lithuania, and southern Estonia are addressed together as the Livonian Basin, characterized by marls and argillaceous limestones. The eastern part of Latvia and Lithuania together with northern Estonia are combined as the Estonian/Lithuanian Shelf, characterized by the shelf limestones (Harris *et al.* 2004).

Conodont stratigraphy of the Sandbian and Katian Stage of Baltoscandia is predominantly based on evolutionary lineage of the genus *Amorphognathus* (Bergström, 2007; Meidla *et al.* 2014). The base of the *A. inaequalis* Conodont Subzone (CSz) is used as the best approximation of the lower boundary of the Sandbian Stage (Bergström *et al.* 2017; Goldman *et al.* 2020). This species is succeeded by the long-ranged *A. tvaerensis* defining a Conodont Zone (CZ) with three CSz based on successive ranges of species of the genus *Baltoniodus*. The younger *A. superbus* defines the next CZ, with the boundary in the lower part of Katian Stage (Bergström *et al.* 2017; Goldman *et al.* 2020). This sequence of conodont zones is also present in sections of the United Kingdom (Bergström & Ferretti, 2018) and the Holy Cross Mountains in Poland (Dzik, 1990).

3. Materials and methods

This study revisits previously a described conodont succession from the Mehikoorma-421 drill core (Männik & Viira, 2005). A detailed core description and distribution of Ordovician conodonts is presented in Põldvere (2005) and Männik & Viira (2005). The Mehikoorma-421 borehole, drilled in the course of geological–hydrogeological mapping in 1972, is located in SE Estonia, on the SW coast of Lake Peipsi (Põldvere, 2005; 58° 14' 34.4" N, 27° 27' 08.3" E; Fig. 1). It penetrates the upper part of the Palaeoproterozoic crystalline basement and spans Ediacaran, Cambrian, Ordovician and Devonian sedimentary rocks, comprising a total thickness of 548.5 m. The studied

Ordovician interval of the core (288–333 m) is represented by various marl and limestones from the Uhaku Regional Stage (RS) (Darriwilian) up to the Oandu RS (Katian) (Fig. 2; Põldvere, 2005). With respect to palaeogeography, the section represents Livonian Basin (Fig. 1) (Harris *et al.* 2004). The study interval is dominated by marl and argillaceous limestone of shelf origin. A geochemical comparison of $\delta^{18}O_{phos}$ and $\delta^{13}C_{carb}$ curves, along with litho- and biostratigraphy from the Mehikoorma core, were published recently (Männik *et al.* 2021), but conodonts from the Mehikoorma core are visualized in only a few samples (Xu *et al.* 2010; Paiste *et al.* 2020).

Conodont samples were collected in 2003/2004, weighing 250–1220 g. All samples yielded conodonts, quite well preserved, with conodont alteration index (CAI) < 1.5. The number of specimens per sample varied from less than 10 up to several thousands, the richest samples coming from the lower part of the succession (Kõrgekallas, Dreimani and Tatruse formations). The studied interval (Fig. 2) includes 45 samples from the depth interval of 288.2–328.6 m, which yielded the elements of *Amorphognathus*. The illustrated specimens are housed in the Institute of Geology at Tallinn University of Technology, Estonia (collection GIT870).

Most representative and intact elements of *Amorphognathus* from all 45 analysed samples were photographed with SEM and partitioned by element types (see online Supplementary Figs S1–S17, available at https://doi.org/10.1017/S0016756822001005) in order to record the full range of changes in morphology of *Amorphognathus* elements in the study interval, and to provide raw data for further taxonomic and stratigraphic analysis. Our identification of taxa is based on empirical comparison of specimens. A statistical approach for species delineation (e.g. Guenser *et al.* 2022) is currently problematic because most Pa elements in our material are only partly preserved.

4. Systematic description

All descriptions below are compiled without considering the positions of conodont elements in the apparatus, as their anatomical
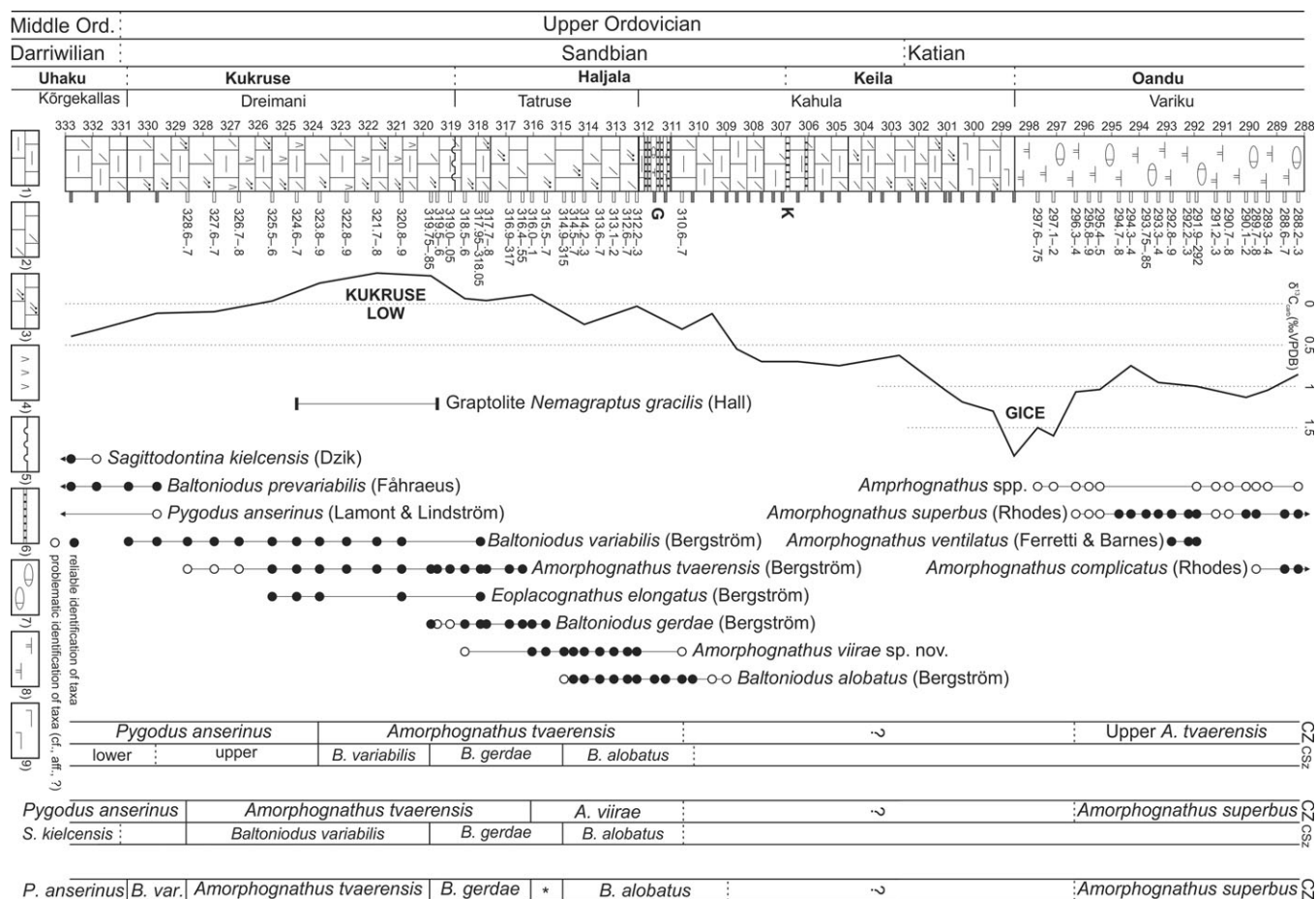
Fig. 2. Distribution of selected conodont taxa in the Sandbian strata of Mehikoorma-421 core section. From left to right: global series, global stage, regional stage, formation, lithological log (after Põldvere, 2005), biostratigraphical samples (hollow boxes, with depth, contained genus *Amorphognathus* elements), δ¹³C$_{carb}$ record (Kaljo *et al.* 2007, table 2; Bergström *et al.* 2009), distribution of the graptolite *Nemagraptus gracilis* after Männik *et al.* (2021), zonation in Männik *et al.* (2021), zonation modified from Webby *et al.* (2004), zonation proposed in this study. Ord. – Ordovician; 1 – argillaceous limestone; 2 – limestone with fine-grained skeletal detritus; 3 – limestone with coarse pyritized skeletal detritus; 4 – kerogen; 5 – discontinuity surface; 6 – bed of altered volcanic ash (K-bentonite); 7 – limestone nodules; 8 – dolomitized marlstone; 9 – calcareous marlstone; lower – *Sagittodontina kielcensis*; upper – *Amorphognathus inaequalis*; * – *Amorphognathus viirae* sp. nov.; K – Kinnekulle K-bentonite; G – Grefsen group K-bentonites (Bergström *et al.* 1995); CZ – conodont zones; CSz – conodont subzones. Lower boundaries of *A. tvaerensis* and *A. superbus* conodont zones are based on appearance of the first M elements of the species.

orientation is not known; biological terminology (ventral, dorsal, caudal etc.) advocated by Purnell *et al.* (2000) therefore could not be adopted. Instead, the traditional Pa, Pb, Pc, M, Sa, Sb, Sc, Sd notation introduced by Sweet & Schönlaub (1975) and modified by Cooper (1975) and Sweet (1981, 1988) has been followed. In descriptions of elements the terms anterior, posterior, lateral, inner, outer, upper and lower are used in the conventional sense for isolated conodont elements (see Sweet, 1981, 1988), and do not refer to biological orientation in the animal. The use of these terms in descriptions of P elements of *Amorphognathus* is illustrated in Figure 3s, t, al and an. The use of cusp, posterior denticle and anterior, posterior and lateral processes in M elements is demonstrated in Figure 3h.

Material count for each species is based on illustrated and/or examined elements of most representative and intact material. Complete amount is higher but not counted.

Genus *Amorphognathus* Branson & Mehl (1933)

Type species. *Amorphognathus ordovicicus* Branson & Mehl (1933).

Diagnosis. Bergström (1971, p. 131–4).

Remarks. Species diagnostics are based on general morphology of the Pa elements and on the features of denticulation on the upper edge of the M element (Ferretti *et al.* 2014a).

Occurrence in the Baltoscandian region: Sandbian–Hirnantian.

Amorphognathus inaequalis (Rhodes, 1953)

1953 *Amorphognathus inaequalis* sp. nov.; Rhodes (1953, p. 283–4, pl. 22: 204).

1974 *Amorphognathus inaequalis* Rhodes (1953); Lindström *et al.* (1974, p. 16–17, pl. 1: 8–11; pl. 2: 1, 2, 7).

1985 *Amorphognathus inaequalis* Rhodes (1953); Bergström & Orchard (1985, pl. 2.2: 14).

1987 *Amorphognathus inaequalis* Rhodes (1953); Bergström *et al.* (1987, pl. 18.1: 8–10).

2022 *Amorphognathus inaequalis* Rhodes (1953); Ferretti & Bergström (2022, p. 467–9, fig. 9A–M).

Diagnosis. Rhodes (1953, p. 283–4).

Remarks. The holotype of *A. inaequalis* (Rhodes, 1953, pl. 22, fig. 204) is a sinistral Pa element. The dextral Pa element, illustrated by Lindström *et al.* (1974, pl. 1, figs 9–11), has an outline similar to that of a sinistral Pa element. Both Pa elements have straight posterior and anterior processes (in upper view), with an angle between them of *c.* 150° for the dextral Pa element and *c.* 165° for the sinistral Pa element. None of the dextral Pa elements of *A. inaequalis* illustrated so far (Lindström *et al.* 1974, pl. 1, figs 9–11; Bergström *et al.* 1987, pl. 18.1, fig. 8; Ferretti & Bergström, 2022,
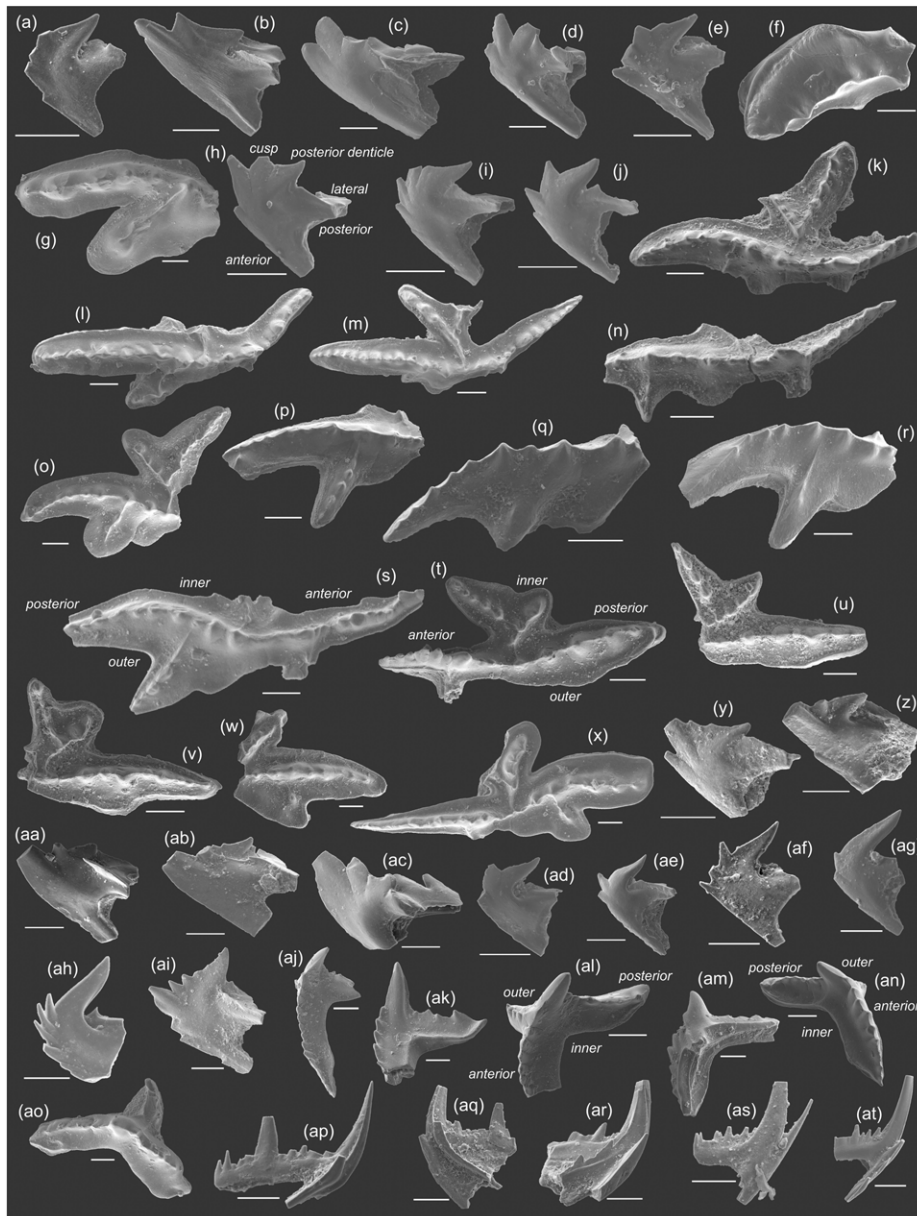
Fig. 3. *Amorphognathus tvaerensis* (Bergström, 1962) elements from the Mehikoorma core: (a) sinistral M element, lateral view, sample 328.6–328.7 m, specimen GIT870-363; (b) dextral M element, lateral view, sample 327.6–327.7 m, specimen GIT870-364; (c) sinistral M element, lateral view, sample 326.6–326.7 m, specimen GIT870-365; (d) sinistral M element, lateral view, sample 325.5–325.6 m, specimen GIT870-366; (e) dextral M element, lateral view, sample 325.5–325.6 m, specimen GIT870-367; (f) probable fragment of dextral Pa element, posterior process, upper view, sample 328.6–328.7 m, specimen GIT870-1; (g) dextral Pa element, posterior process, upper view, sample 325.5–325.6 m, specimen GIT870-4; (h) sinistral M element, lateral view, sample 324.6–324.7 m, specimen GIT870-370; (i) sinistral M element, lateral view, sample 324.6–324.7 m, specimen GIT870-375; (j) sinistral M element, lateral view, sample 324.6–324.7 m, specimen GIT870-376; (k) dextral Pa element, upper view, sample 320.8–320.9 m, specimen GIT870-30; (l) dextral Pa element, upper view, sample 319.5–319.6 m, specimen GIT870-44; (m) dextral Pa element, upper view, sample 316.4–316.55 m, specimen GIT870-82; (n) dextral Pa element, upper view, sample 323.8–323.9 m, specimen GIT870-14; (o) dextral Pa element, posterior process, upper view, sample 319.0–319.05 m, specimen GIT870-51; (p) dextral Pa element, posterior process, upper view, sample 319.75–319.85 m, specimen GIT870-36; (q) dextral Pa element, posterior process, upper view, sample 322.8–322.9 m, specimen GIT870-20; (r) dextral Pa element, posterior process, upper view, sample 316.9–317 m, specimen GIT870-72; (s) dextral Pa element, upper view, sample 316.4–316.55 m, specimen GIT870-79; (t) sinistral Pa element, upper view, sample 323.8–323.9 m, specimen GIT870-17; (u) Pa element, posterior process, upper view, sample 323.8–323.9 m, specimen GIT870-18; (v) sinistral Pa element, posterior process, upper view, sample 320.8–320.9 m, specimen GIT870-34; (w) sinistral Pa element, posterior process, upper view, sample 319.75–319.85 m, specimen GIT870-39; (x) sinistral Pa element, upper view, sample 316.4–316.55 m, specimen GIT870-85; (y) sinistral M element, lateral view, sample 323.8–323.9 m, specimen GIT870-377; (z) dextral M element, lateral view, sample 323.8–323.9 m, specimen GIT870-379; (aa) dextral M element, lateral view, sample 319.75–319.85 m, specimen GIT870-406; (ab) dextral M element, lateral view, sample 319.75–319.85 m, specimen GIT870-408; (ac) sinistral M element, lateral view, sample 317.95–318.05 m, specimen GIT870-451; (ad) dextral M element, lateral view, sample 324.6–324.7 m, specimen GIT870-373; (ae) sinistral M element, lateral view, sample 321.7–321.8 m, specimen GIT870-396; (af) dextral M element, lateral view, sample 319.75–319.85 m, specimen GIT870-413; (ag) sinistral M element, lateral view, sample 316.9–317 m, specimen GIT870-476; (ah) sinistral M element, lateral view, sample 316.4–316.55 m, specimen GIT870-486; (ai) dextral M element, lateral view, sample 317.7–317.8 m, specimen GIT870-460; (aj) dextral Pb element, upper view, sample 323.8–323.9 m, specimen GIT870-250; (ak) dextral Pb element, inner-lateral view, sample 323.8–323.9 m, specimen GIT870-251; (al) dextral Pb element, upper view, sample 320.8–320.9 m, specimen GIT870-260; (am) sinistral Pb element, outer-lateral view, sample 320.8–320.9 m, specimen GIT870-257; (an) sinistral Pb element, upper view, sample 321.7–321.8 m, specimen GIT870-255; (ao) sinistral Pb element, upper view, sample 319.5–319.6 m, specimen GIT870-266; (ap) Sa element, lateral view, sample 324.6–324.7 m, specimen GIT870-622; (aq) Sd element, lateral view, sample 323.8–323.9 m, specimen GIT870-623; (ar) Sb element, lateral view, sample 317.7–317.8 m, specimen GIT870-655; (as) Sc element, lateral view, sample 318.5–318.6 m, specimen GIT870-649; (at) Sc element, lateral view, sample 319.5–319.6 m, specimen GIT870-644. All scale bars are 100 μm.

pl. 9, figs A, B) have an extra postero-lateral process on the outer side as is known in the dextral Pa elements of the younger species, *A. tvaerensis*. Additionally, both Pa elements of *A. tvaerensis* have a slight curvature on the posterior process (Ferretti & Bergström, 2022, pl. 11, figs B, C), while no recognizable curvature is recognized in *A. inaequalis* (Ferretti & Bergström, 2022, pl. 9, figs A, C). While the Pb and S elements of *A. inaequalis* are similar to those of younger species of *Amorphognathus* (Ferretti & Bergström, 2022), the M element can be differentiated mainly by lack of a prominent posteriorly directed denticle, which is characteristic of the M element of *A. tvaerensis*. However, the illustrated M elements of *A. inaequalis* are broken (Bergström *et al.* 1987, pl. 18.1, fig. 10; Ferretti & Bergström, 2022, fig. 9J, K) or shown in lateral view only (Lindström *et al.* 1974, pl. 2, fig. 7), making it difficult to determine their actual outline. The Pa elements provide the best opportunity to identify *A. inaequalis* with certainty, and differentiate it from *A. tvaerensis*. A probable dextral Pa element that has intermediate morphology between those of *A. inaequalis* and *A. tvaerensis* is figured by Ferretti & Bergström (2022, fig. 11D). This is the oldest specimen in this section that bears an extra postero-lateral process on the outer side, a small lateral expansion next to it and a weak sinusoidal curvature in the main row of denticles.

Specimens identified in an earlier study as *A. inaequalis* (Dzik, 1976, fig. 27a–f) were later attributed to an earlier form of *A. tvaerensis* (Dzik, 1994). Likewise, Viira (2008) stated that the earliest M elements of *A. tvaerensis* are very similar to those of *A. inaequalis*, as both have a larger straight anteriorly directed denticle on the anterior end. Published illustrations of *A. inaequalis* are very rare; no specimens are figured from the Baltoscandian sections so far, although both Swedish (Bergström, 2007) and Estonian (Meidla *et al.* 2014) papers contain references to the *A. inaequalis* CSz underlying the *A. tvaerensis* CZ.

According to Ferretti & Bergström (2022, table 1), *A. inaequalis* occurs together with *Baltoniodus prevariabilis*. However, some images of the specimens of *B. prevariabilis* provided by Ferretti & Bergström (2022, fig. 8M, N) from the samples, including also *A. inaequalis*, appear quite similar to *B. variabilis*. Specifically, the main feature of *B. variabilis*, the 'prominent triangular lateral expansion of the inner side of the posterior process' (Bergström, 1971, p. 148), is present in these specimens, making them distinct from the element illustrated next to them (Ferretti & Bergstrom, 2022, fig. 8O), representing a typical *B. prevariabilis* with no triangular lateral expansion. This indicates that *A. inaequalis* probably has a longer range and also occurs together with *B. variablis*. In the Mehikoorma core section, the lowermost elements of *Amorphognathus* have been found from the interval corresponding to the *B. variabilis* range in the Mehikoorma core, and none of the Pa elements occurring here can be assigned to *A. inaequalis*. The lowermost M elements of *Amorphognathus* in the studied interval of this section (samples from interval 325.5–328.7 m, Fig. 3a–e) are typical *A. tvaerensis*. Pa elements (depth 325.5–328.7 m, Fig. 3f, g) with curvature on the posterior process at the same depth supports the latter. The only single M element in the Mehikoorma section that was earlier identified as *A. inaequalis* by Männik & Viira (2005; sample 327.6–327.7 m, Fig. 3b) has two anteriorly directed denticles with a larger denticle as the anteriormost and a small posteriorly directed one. A morphologically somewhat similar M element is also present a few samples higher in the section (sample 324.6–324.7 m, Fig. 3h). As Pa elements indicative of *A. inaequalis* have not been found in these samples both M elements are tentatively attributed to *A. tvaerensis*, and the strata corresponding to the range interval of *A. inaequalis*

(326.6–324.6 m) in the sense of Viira (2008, fig. 7) are here attributed to the *A. tvaerensis* CZ as its lower part.

From comparison of the first *Amorphognathus* elements in the Mehikoorma, Ruhnu (Männik, 2003) and Velise (Paiste *et al.* 2022) drill cores of Estonia, and in the Fjäcka main section and in the Smedsby Gård drillcore in Sweden, along with a personal communication (S. M. Bergström, 2022), it is evident that there is currently no evidence that *A. inaequalis* could be present in Estonian or Swedish sections. It is therefore likely that *A. inaequalis* was not present on the Baltica Palaeocontinent during early Sandbian time. *A. inaequalis* has been reported from the Bliudziai-150 drillcore in Lithuania (Stouge *et al.* 2016) and the Kovel-1 drillcore in Ukraine (Saadre *et al.* 2004), but no specimen was illustrated making it impossible to check these indentifications.

Distribution. South Wales (Ffairfeach, Golden Grove, Dynevor Park), Flags and Grits Formation, Llandeilo flags (uppermost Darriwilian, lowermost Sandbian, Ferretti & Bergström, 2022); West France (Armorican Massif): Upper Postolonnec Formation (Sandbian or Darriwilian, Lindström *et al.* 1974).

Amorphognathus tvaerensis Bergström (1962)

1962 *Amorphognathus tvaerensis* sp. nov.; Bergström (1962, p. 36–7, pl. 4: 7–10).

1962 *Amorphognathus ordovicica* Branson & Mehl ssp. *simplicior* spp. nov.; Bergström (1962, p. 34–5, pl. 4: 2, 5, 6).

1971 *Amorphognathus tvaerensis* Bergström (1962); Bergström (1971, p. 135–6, pl. 2: 10–11).

1971 *Amorphognathus tvaerensis* Bergström (1962); Sweet *et al.* (1971, pl. 1: 24).

1974 *Amorphognathus ordovicica* spp. nov. 3.; Viira (1974, p. 59, 60, pl. 7: 23, not including 18, 19, 24).

1976 *Amorphognathus inaequalis* Rhodes (1953); Dzik (1976, fig. 27c–f).

1976 *Amorphognathus tvaerensis* Bergström (1962); Dzik (1976, fig. 27g–q).

1981 *Amorphognathus tvaerensis* Bergström (1962); Nowlan (1981, p. 11, pl. 5: 13, 14, 16).

1985 *Amorphognathus tvaerensis* Bergström (1962); Bergström & Orchard (1985, pl. 2.3: 8, 9, 11, 16).

1994 *Amorphognathus tvaerensis* Bergström (1962); Dzik (1994, p. 91–3, pl. 22: 8–22; pl. 23: 1, 2).

?2000 *Amorphognathus tvaerensis* Bergström (1962); Leslie (2000, fig. 7: 14–19).

2006 *Amorphognathus tvaerensis* Bergström (1962); Viira *et al.* (2006, p. 223–5, fig. 1: 1–9, 11, 13–15).

2008 *Amorphognathus tvaerensis* Bergström (1962); Viira (2008, p. 35, 36, fig. 5A–I, O–R, not including J, K, L, M, N; fig. 6A–E, G–I, not including F; fig. 8A–S).

2016 *Amorphognathus tvaerensis* Bergström (1962); Stouge *et al.* (2016, fig. 3E, J, K, Q, R).

?2018 *Amorphognathus* cf. *A. tvaerensis* Bergström (1962); Bergström & Ferretti (2018, fig. 6g–n).

2020 *Amorphognathus tvaerensis* Bergström (1962); Paiste *et al.* (2020, fig. 4E, F, not including A–D; fig. 5A–D).

2022 *Amorphognathus tvaerensis* Bergström (1962); Ferretti & Bergström (2022, p. 8–14, pl. 11: A–W).

2022 *Amorphognathus tvaerensis* Bergström (1962); Paiste *et al.* (2022, fig. 4A–C, H–J, M–Q, S–U, Y–AG, AO–AU, AW, not including D–G, K, L, R, V–X, AH–AN, AV).

Diagnosis. Bergström (1971, p. 135–6).

Remarks. Detailed description of the dextral Pa holotype and paired sinistral Pa element (designated as *A. ordovicica* ssp. *simplicior*) are provided by Bergström (1962), and the multi-element

species is discussed by Bergström (1971). The main difference from the younger species of *Amorphognathus*, *A. superbus*, is the occurrence of an extra (second) postero-lateral process on the outer side of the dextral Pa element that is missing in the same element of *A. superbus* (Bergström, 1971). This extra process also has a small lateral anterior lobe next to it, originally described as ' . . . a slight curvature outwards of the aboral margin which might be interpreted as a rudimentary development of a new process . . . ' (Bergström, 1962, p. 37). A typical M element of *A. tvaerensis* has a characteristic prominent reclined posteriorly directed denticle of variable size located posteriorly of usually poorly developed, and often indistinguishable in size from, other denticles cusp (Bergström, 1971, pl. 2, fig. 11). This characteristic denticle (referred to here as posterior denticle) gradually disappears and the cusp becomes dominant in younger species, in *A. superbus* and *A. ordovicicus* (Bergström, 1971, pl. 2, figs 7, 9).

The lowermost dextral Pa element with features characteristic of *A. tvaerensis* in the Mehikoorma section comes from the interval 325.5–326.6 m (Fig. 3g). It is a posterior process of a broken dextral Pa element with the characteristic sinusoidal curvature in the main row of denticles and with a postero-lateral process. However, all three lower samples from the interval 328.7–326.7 m yield M elements that are characteristic of *A. tvaerensis* (Fig. 3a–c), and mark the probable first appearance of *A. tvaerensis* in the Mehikoorma section at 328.7 m. The elements of *A. tvaerensis* range in the Mehikoorma section up to depth 316.4 m.

Variation of *A. tvaerensis* is prominent in Pa (online Supplementary Figs S1a–ai; S2a–u, w–aq; S3a–i), Pb (online Supplementary Fig. S7a–ax) and M elements (online Supplementary Figs S9 a–az; S10a–s, ab–bb; S11a–s), but S elements (online Supplementary Fig. S14a–bd) show no significant variation. While the sinusoidal outline of the dextral Pa element in the upper view is a characteristic feature of *A. tvaerensis* (Fig. 3k), a few samples also yielded elements with almost straight posterior process (Fig. 3l, m). All these specimens come from the upper part of the *A. tvaerensis* range, from the *B. gerdae* CSz, and are similar to the specimen illustrated by Bergström & Orchard (1985, pl. 2.3, fig. 11) from the Girvan area, southern Scotland. Configuration of the extra postero-lateral process is highly variable. The length of it can change from a small node (Fig. 3n) or bulge (Fig. 3o) to a prominent process (Fig. 3p), while denticulation on it may be absent (Fig. 3q), rudimentary (in a form of ridge; Fig. 3r) or prominent (Fig. 3p). The small anterior lobe next to the extra postero-lateral process is usually merged to the process (Fig. 3s) but, occasionally, may be located separately (Fig. 3n). Sinistral Pa elements of *A. tvaerensis* in the lowermost samples show no clearly recognizable lateral expansion on the outer side of its posterior process (Fig. 3t, u), but it appears on elements from the uppermost *B. variabilis* CSz (Fig. 3v). In the lowermost *B. gerdae* CSz, the lateral expansion on the sinistral Pa elements becomes prominent (Fig. 3w) and this feature is present throughout the upper range of *A. tvaerensis*. The youngest sinistral Pa elements of *A. tvaerensis* also show additional denticulation on that lateral expansion (Fig. 3x).

The variation of M elements is expressed in the changing number of anteriorly oriented denticles, including cusp and orientation of the prominent posterior denticle. Previously described morphotypes of M elements in *A. tvaerensis* (Viira, 2008) are also present in Mehikoorma section. However, their proposed stratigraphic importance is not evident. The first morphotype is described as ' . . . low in the range of *A. tvaerensis*, is similar to *A. inaequalis* . . . ' and ' . . . has a large straight denticle in the anterior part of the oral

denticle row . . . ' (Viira, 2008, p. 36, fig. 8C). Another morphotype is similar to the third described as ' . . . late specimens of *A. tvaerensis* is characterized by an orally directed large denticle in the anterior part and occurs on the level of the *B. gerdae* range . . . ' (Viira, 2008, p. 36, figs 5K, 8Q). M elements that fit with the previous descriptions (Viira, 2008, figs 5K, 8C, Q) are present from the lower part of *A. tvaerensis* range (Fig. 3b), in the *B. alobatus* CSz (Fig. 3h, y, z), in the lower part of the *B. gerdae* CSz (Fig. 3aa, ab) and within the uppermost range of *A. tvaerensis* (Fig. 3a, c). Similarly, the proposed second morphotype described as ' . . . with a very characteristic posteriorly directed denticle in the M element occurs in the middle part of the *A. tvaerensis* range . . . ' (Viira, 2008, p. 36, figs 5E, 8H) is present in almost every sample from the *B. alobatus* CSz (Fig. 3a, e, i, ad, ae), from the lower *B. gerdae* CSz (Fig. 3af) and from the upper range of *A. tvaerensis* (Fig. 3ag, ah).

The prominently reclined posterior denticle of variable size of the M element between the denticle and the posterior processes forms an angle of *c.* 50° within *B. variabilis* CSz (Fig. 3e, i, ad) and *c.* 75° within *B. gerdae* CSz (Fig. 3af, ah). No stratigraphic significance is found within the change of the number of anteriorly directed denticles. The number of these denticles ranges from two (Fig. 3b, ag) up to four or more (Fig. 3ah, ai) varying in size.

No distinct variation pattern is recognized in Pb elements (Fig. 3aj–ao; online Supplementary Fig. S7a–ax) and S elements (Fig. 3ap–at; online Supplementary Fig. S14a–bd) of *A. tvaerensis*.

Material. Mehikoorma section: 47 dextral Pa, 33 sinistral Pa, 25 dextral Pb, 23 sinistral Pb, 118 M and about 200 S elements; Velise section: 10 dextral Pa, 4 sinistral Pa, 5 dextral Pb, 5 sinistral Pb, 28 M and about 100 S elements; Ruhnu section: 11 dextral Pa, 9 sinistral Pa, 9 dextral Pb, 10 sinistral Pb, 20 M and about 80 S elements; Fjäcka Main section: 14 dextral Pa, 12 sinistral Pa, 12 dextral Pb, 11 sinistral Pb, 8 M and about 60 S elements; Smedsby Gård drillcore: 20 dextral Pa, 12 sinistral Pa, 14 dextral Pb, 10 sinistral Pb, 14 M and about 50 S elements.

Distribution. Baltoscandian region: lower half of the Sandbian; Fjäcka Main section: Dalby limestone (6.05–13.10 m above the base of Dalby limestone); Mehikoorma section: Dreimani and Tatruse Formation (316.4–328.7 m); Ruhnu section: Dreimani and Adze Formation (653.8–662.8 m); Smedsby Gård drillcore: Dalby limestone (95.35–130.49 m); Velise section: Pihla and Tatruse Formation (202.95–211.83 m).

Amorphognathus viirae sp. nov.

1974 *Amorphognathus ordovicica* spp. nov. 1.; Viira (1974, p. 59–60, pl. 7: 15, 16).

1974 *Amorphognathus ordovicica* spp. nov. 2.; Viira (1974, p. 59–60, pl. 7: 17, 20–22).

1974 *Amorphognathus ordovicica* spp. nov. 3.; Viira (1974, p. 59–60, pl. 7: 18, 19, 24, not including 23).

1990 *Amorphognathus superbus* Rhodes (1953); Dzik (1990, p. 24, text-figs 16, 17: depth 2–3 m).

1994 *Amorphognathus superbus* Rhodes (1953); Dzik (1994, p. 93, 94, pl. 23: 3–5; text-fig. 22: samples 93–96).

1999a *Amorphognathus* aff. *ventilatus* Ferretti & Barnes (1997); Dzik (1999a, pl. 1: 1–21).

1999a *Amorphognathus tvaerensis* Bergström (1962); Dzik (1999a, pl. 1: 22–26).

1999b *Amorphognathus tvaerensis* Bergström (1962); Dzik (1999b, text-fig. 5: depth 1.5–2.5 m).

?2007 *Amorphognathus tvaerensis* Bergström (1962); Goldman *et al.* (2007, fig. 7: 17–22).

2008 *Amorphognathus tvaerensis* Bergström (1962); Viira (2008, fig. 5J, K, L, M, N, not including A–I, O–R; fig. 6F, not including A–E, G–I; not including fig. 8A–S).

2020 *Amorphognathus tvaerensis* Bergström (1962); Paiste *et al.* (2020, fig. 4A–D, not including E, F; not including fig. 5A–D).

2022 *Amorphognathus tvaerensis* Bergström (1962); Paiste *et al.* (2022, fig. 4D–G, K, L, R, V–X, AH–AN, AV, not including A–C, H–J, M–Q, S–U, Y–AG, AO–AU, AW).

Holotype. GIT870-99 (Fig. 4a), from Mehikoorma-421 core section sample 314.9–315 m, Tatruse Formation, Sandbian Stage, Upper Ordovician, Estonia.

Etymology. The species is named after conodont specialist Viive Viira who published the first illustrations of this new species (Viira, 1974).

Diagnosis. A species of *Amorphognathus* in which the main denticle row on the dextral Pa element in upper view is shaped as sinuous curve. A small and distinct lateral lobe occurs on the outer side of the posterior process, at the starting point of the sinuous curvature. The element bears bifurcated lateral processes on both sides.

Description. Dextral Pa element. Inner lateral process is connected to the main blade just posteriorly of the cusp, at the starting point of the sinuous curvature (Fig. 4a). The shorter (posterior) branch of the process is almost perpendicular to the main row of denticles. The longer, anterior branch (at least twice as long the posterior branch) is directed away from the anterior process at an angle of *c.* 40°. The bifurcated outer lateral process is smaller than the inner process and is positioned just anteriorly of the cusp (Fig. 4b, c). In all available specimens this process is only partly preserved but, as much as is visible, its posterior branch seems to be longer than the anterior branch. The anterior process of the dextral Pa element is straight in upper view (Fig. 4a) and tilted somewhat downwards (at *c.* 25°) in lateral view (Fig. 4c). The posterior process is slightly arched in lateral view. A distinct higher denticle (smaller than the cusp) is positioned in the proximal part of the main row of denticles on the posterior process, just above the small platform on its outer side at the beginning of the sinuous curvature. A distinct rim surrounds the basal platform of the element (Fig. 4c). The basal cavity is wide and deep below the posterior and lateral processes, but narrows sharply below the anterior process and continues as a narrow groove up to its distal end (Fig. 4d). The variation in morphology of the dextral Pa element (online Supplementary Figs S2v; S3j–m, o, q, r, u–w, aa, ab, ae–ag; S4a–c, g–j, n–q, w–z) is mainly expressed in configuration of its posterior process. In upper view, the distal end of it may be located in the line of the anterior process (Fig. 4a) or turned outwards (Fig. 4b). Additionally, a few elements bear a single denticle on the small outer platform lobe (Fig. 4b, e). Some elements studied bear a quite distinct lateral expansion on the inner sides of their posterior processes. This feature appears sporadically at different levels in the species' range interval: in the lowermost sample studied (Fig. 4f), in the middle part of the range (Fig. 4g) and also in its upper part (Fig. 4h). A probable juvenile example of a dextral Pa element (Fig. 4i) has slender processes with no lateral expansion or clearly developed lateral lobe on the outer side of the posterior process.

The sinistral Pa element is a platform element with predominantly straight (Fig. 4j) or slightly curved (Fig. 4k) main row of denticles. The element bears a bifurcated lateral process on both sides. The inner lateral process joins the main blade somewhat posteriorly of the cusp (Fig. 4k). Its anterior branch is twice as long or even slightly longer than posterior branch. Branches of the outer

lateral process located just below the cusp are about the same size (Fig. 4l). Similarly to the dextral Pa element, the anterior process of the sinistral Pa is tilted downwards and a distinct rim surrounds its basal platform (Fig. 4k, m). The main variation in morphology of the sinistral Pa element (online Supplementary Figs S3n, p, s, t, x–z, ac, ad, ah, ai; S4d–f, k–m, r–v, aa–ac) is related to the width of the basal platform below its posterior process that is narrower on specimens from older samples (Fig. 4j, k, n) and becomes wider on those from younger samples (Fig. 4o). The small outer lateral expansion on its posterior process becomes more common on specimens from younger samples (Fig. 4l, p).

The dextral Pb element is dominated by a conspicuous central suberect pointed cusp (Fig. 4q) with three diverging denticulated processes (Fig. 4r). The posterior process is straight, with a slightly curved to inner side row of denticles and a distinct basal lateral expansion (Fig. 4s). The outline of this expansion is wavy in lateral view (Fig. 4q). The angle between the downwards oriented anterior process and posterior process is *c.* 90°. The anterior process is bent to inner side, crosswise to posterior process (Fig. 4t), slightly longer than the posterior process and with an inner edge and pointed end (Fig. 4u). The outer lateral process is short and emerges with anterior process just below the cusp (Fig. 4v). This short process bears 1–3 discrete pointed denticles and is laterally compressed. The cusp of the dextral Pb element (Fig. 4q) is twice as high as that of the sinistral Pb element (Fig. 4w). No significant variation in morphology of the dextral Pb element was found (online Supplementary Figs S7az, ba, bd–bf, bi, bj, bm; S8c, f, g, l, m).

The sinistral Pb element resembles its dextral counterpart and differs in only a few noticeable ways. The cusp of the sinistral Pb (Fig. 4w) is smaller in size compared with the dextral Pb (Fig. 4t), and the angle between the downwards directed anterior process and posterior process is *c.* 120° (Fig. 4x). Additionally, both posterior and anterior process are of a similar length and possess basal lateral expansions. No significant variation in morphology of the sinistral Pb element was found (online Supplementary Figs S7ay, bc, bg, bh, bk, bl; S8a, b, d, e, h–k).

The M element is characterized by three variously denticulated processes. The anterior edge of the anterior process is sharp, rarely denticulated and may bear a different number (usually 2–5) of anteriorly directed denticles (Fig. 4y–ai). Cusp (interpreted here as the first prominent denticle anterior to the posterior denticle) may be prominent (Fig. 4y) or undistingushable in size (Fig. 4ae, ag). The backwards directed posterior denticle on the proximal part of the posterior process also varies greatly in size but, as a rule, is very prominent, sharply turned backwards, and with its distal end curved anteriorly (Fig. 4ac, af–ai). The posterior process is usually poorly denticulated (Fig. 4ab, ad) and form an angle of *c.* 40° with the anterior process. The inner lateral process is directed at an angle of *c.* 45° with the posterior process. Rare denticles occur in the distal part of the lateral process. All processes are sharp-edged and bear ridges (keels) between denticles. The number, size and location of denticles on their anterior end of M element vary greatly (online Supplementary Figs S10t–aa; S11t–ba; S12a–av), for example, from specimens with almost unrecognizeable posterior denticle (Fig. 4ab) to those with a very distinct denticle (Fig. 4ac, af–ai), and from those with only two larger denticles on the anterior process (Fig. 4ae, ai) to those with several (Fig. 4y, ag, ah). Additionally, the denticle and the posterior processes form an angle of *c.* 90° (Fig. 4z, aa) in older specimens and *c.* 110° in younger specimens (Fig. 4ah, ai). The latter variation described in the studied section seems to have stratigraphic value,
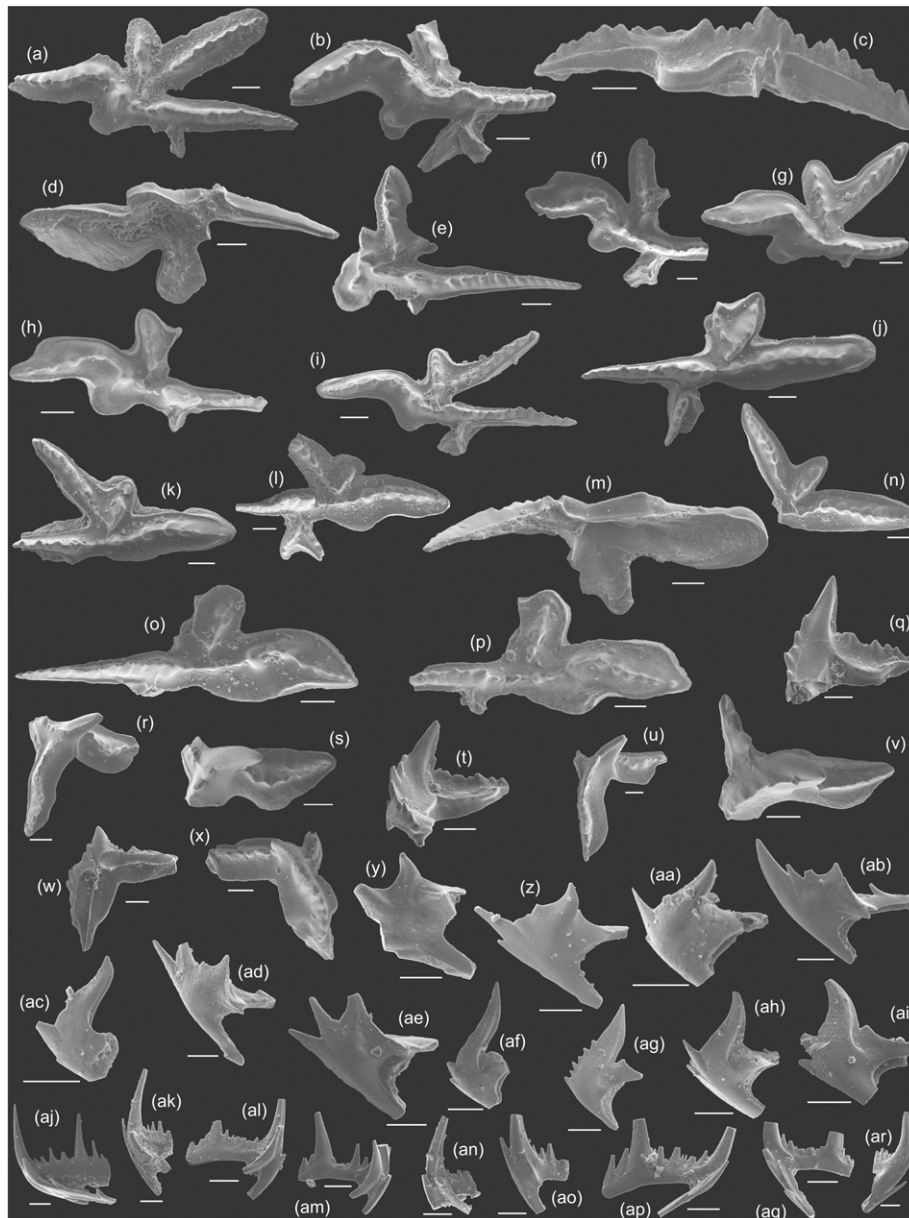
Fig. 4. *Amorphognathus viirae* sp. nov. elements from the Mehikoorma core: (a) holotype, dextral Pa element, upper view, sample 314.9–315 m, specimen GIT870-99; (b) dextral Pa element, upper view, sample 315.5–315.7 m, specimen GIT870-95; (c) dextral Pa element, outer-lateral view, sample 313.1–313.2 m, specimen GIT870-121; (d) dextral Pa element, lower view, sample 312.6–312.7 m, specimen GIT870-128; (e) dextral Pa element, upper view, sample 312.6–312.7 m, specimen GIT870-130; (f) dextral Pa element, upper view, sample 316.0–316.1 m, specimen GIT870-90; (g) dextral Pa element, upper view, sample 314.9–315 m, specimen GIT870-101; (h) dextral Pa element, upper view, sample 313.1–313.2 m, specimen GIT870-120; (i) dextral Pa element, upper view, sample 313.1–313.2 m, specimen GIT870-123; (j) sinistral Pa element, upper view, sample 315.5–315.7 m, specimen GIT870-97; (k) sinistral Pa element, upper view, sample 312.6–312.7 m, specimen GIT870-135; (l) sinistral Pa element, upper view, sample 312.2–312.3 m, specimen GIT870-140; (m) sinistral Pa element, lower view, sample 312.6–312.7 m, specimen GIT870-134; (n) sinistral Pa element, posterior process, upper view, sample 313.6–313.7 m, specimen GIT870-117; (o) sinistral Pa element, upper view, sample 312.6–312.7 m, specimen GIT870-131; (p) sinistral Pa element, upper view, sample 313.1–313.2 m, specimen GIT870-126; (q) dextral Pb element, inner-lateral view, sample 316.0–316.1 m, specimen GIT870-288; (r) dextral Pb element, upper view, sample 316.0–316.1 m, specimen GIT870-289; (s) dextral Pb element, upper view, sample 312.2–312.3 m, specimen GIT870-314; (t) dextral Pb element, inner-lateral view, sample 314.9–315 m, specimen GIT870-292; (u) dextral Pb element, upper view, sample 314.9–315 m, specimen GIT870-293; (v) dextral Pb element, upper view, sample 314.9–315 m, specimen GIT870-294; (w) sinistral Pb element, outer-lateral view, sample 313.1–313.2 m, specimen GIT870-305; (x) sinistral Pb element, upper view, sample 314.2–314.3 m, specimen GIT870-300; (y) dextral M element, lateral view, sample 316.0–316.1 m, specimen GIT870-489; (z) sinistral M element, lateral view, sample 315.5–315.7 m, specimen GIT870-497; (aa) sinistral M element, lateral view, sample 314.9–315 m, specimen GIT870-512; (ab) sinistral M element, lateral view, sample 314.2–314.3 m, specimen GIT870-522; (ac) sinistral M element, lateral view, sample 313.6–313.7 m, specimen GIT870-537; (ad) sinistral M element, lateral view, sample 313.1–313.2 m, specimen GIT870-538; (ae) sinistral M element, lateral view, sample 312.6–312.7 m, specimen GIT870-550; (af) sinistral M element, lateral view, sample 312.6–312.7 m, specimen GIT870-558; (ag) sinistral M element, lateral view, sample 312.6–312.7 m, specimen GIT870-559; (ah) sinistral M element, lateral view, sample 312.2–312.3 m, specimen GIT870-566; (ai) sinistral M element, lateral view, sample 312.2–312.3 m, specimen GIT870-568; (aj) Sa element, lateral view, sample 312.6–312.7 m, specimen GIT870-705; (ak) Sd element, lateral view, sample 312.2–312.3 m, specimen GIT870-711; (al) Sb element, lateral view, sample 312.2–312.3 m, specimen GIT870-712; (am) Sb element, lateral view, sample 314.2–314.3 m, specimen GIT870-691; (an) Sd element, lateral view, sample 312.2–312.3 m, specimen GIT870-710; (ao) Sc element, lateral view, sample 312.2–312.3 m, specimen GIT870-717; (ap) Sc element, lateral view, sample 312.2–312.3 m, specimen GIT870-718; (aq) Sc element, lateral view, sample 313.6–313.7 m, specimen GIT870-699; (ar) Sc element, lateral view, sample 314.2–314.3 m, specimen GIT870-696. All scale bars are 100 µm.

allowing the older and younger populations of *A. viirae* sp. nov. to be distinguished.

The S elements of *A. viirae* sp. nov. (Fig. 4aj–ar; online Supplementary Figs S14be–bu; S15a–ag) are typical of the genus *Amorphognathus* and similar to those in the apparatus of its ancestor *A. tvaerensis* (Fig. 3ap–at). No significant differences in their morphology could be noted. However, some noticeable differences were present within Sc elements. The orientation of the cusp varies from proclined (Fig. 4ao–ap) to erect (Fig. 4aq–ar). Denticulation on the anterior process may vary from rare denticles (Fig. 4ao–ap) up to a row containing numerous denticles (Fig. 4aq–ar). A bulge on the outer side of the element between the posterior and anterior processes may be visible (Fig. 4ao), but the same area can also be round and smooth (Fig. 4ar).

Comparison. The absence of an extra postero-lateral process on the outer side of dextral Pa element was the main distinguishing feature for erecting *A. viirae* sp. nov. as a new species and differentiating it from its predecessor *A. tvaerensis*. This process is one of the main characteristic features of the dextral Pa element of *A. tvaerensis*, and its absence has been used previously for differentiating dextral Pa elements of *A. superbus*. The small lateral lobe anterior to the extra postero-lateral process in the dextral Pa element of *A. tvaerensis* (Fig. 3s) persists in dextral Pa elements of *A. viirae* sp. nov. (Fig. 4a).

The main central row of denticles is shaped as sinuous curve in both *A. tvaerensis* and *A. viirae* sp. nov.; the curvature is smooth in elements of *A. tvaerensis* (Fig. 3k) but considerably much more distinct in *A. viirae* sp. nov., in which it resembles a cubic function (Fig. 4a). Both Pa elements of *A. viirae* sp. nov. have distinctly longer anterior branches on their inner lateral processes (Fig. 4a, k) than the elements of *A. tvaerensis* (Fig. 3k, t). Additionally, the anterior part of the posterior process (in front of the cusp) is aligned in a straight line with the anterior proccess (Fig. 4a) in dextral Pa elements of *A. viirae* sp. nov., while there is a curvature in this part of the posterior process in *A. tvaerensis* (Fig. 3k).

Pb elements of these two species are almost identical, with the only subtle differences in morphology of the dextral Pb elements. The posterior process in the dextral Pb element of *A. tvaerensis* bears a straight row of denticles (Fig. 3al), while it is slightly curved inwards just behind the cusp in *A. viirae* sp. nov. (Fig. 4s). A narrow basal platform-like edge is present in the posterior processes of both species. Additionally, elements of *A. viirae* sp. nov. possess a distinctive inner lateral expansion (Fig. 4s) that in lateral view has a wavy outline (Fig. 4q). The anterior process of the sinistral Pb element of *A. viirae* sp. nov. bears narrow basal platform ledges on both sides of the denticle row (Fig. 4x), while no noticeable outwards extensions are present on analogous elements of *A. tvaerensis* (Fig. 3ao).

The M elements of *A. viirae* sp. nov. and *A. tvaerensis* are morphologically very similar. The most distinct difference is related to the configuration of their posterior denticle: on elements of *A. viirae* sp. nov. the distal part of it is erect or curved anteriorly (Fig. 4z), while on elements of *A. tvaerensis* it is reclined (Fig. 3af, y). The processes of the M element in *A. tvaerensis* also often tends to be more densely denticulated than those of *A. viirae* sp. nov. but, as a rule, this feature becomes apparent in a comparison with larger samples in which M elements are well represented.

A detailed comparison of *A. viirae* sp. nov. with younger species of *Amorphognathus* is problematic based on material from the Mehikoorma core section. In the upper part of the studied interval, above the range of *A. viirae* sp. nov., *Amorphognathus* is missing or represented by rare, poorly preserved specimens.

This phenomenon is characteristic of the upper Sandbian – lower Katian interval in Baltoscandian sections (Bergström, 2007; Viira, 2008). However, based on published data, some comparisons are still possible.

The dextral Pa element of *A. superbus* shows a relatively straight main row of denticles with the tip of the posterior process turned to the outer side (Bergström, 1971, pl. 2, fig. 8; Dzik, 1976, fig. 28a; Goldman *et al.* 2007, fig. 7: 15), while *A. viirae* sp. nov. has a recognizable sinuous curve in the central part of the main row of denticles (Fig. 4a). Additionally, no extra postero-lateral process (or lateral lobe) on the outer side of the posterior process is present in the dextral Pa elements of *A. superbus*. Furthermore, the posterior branch of inner bifurcated processes of the dextral Pa element of *A. superbus* is considerably shorter than the anterior process (difference 4–5 times) than in *A. viirae* sp. nov. (only 2–3 times). In *A. complicatus* (Rhodes, 1953) the inner lateral process is simple, without a second branch. The posterior process on sinistral Pa element of *A. viirae* sp. nov is 2–3 times longer than the anterior process, while its size difference in younger *A. superbus* and *A. complicatus* decreases and is only *c.* 1.5 times (Dzik, 1976, fig. 28g; Goldman *et al.* 2007, fig. 7: 16). The dextral Pb element of *A. superbus* lacks the slight curvature of denticle row towards the inner side of the posterior process and the distinctive inner basal platform-like lobe (Fig. 5q–s) recognized in elements of *A. viirae* sp. nov. Additionally, the basal platform on the inner side of the posterior process of the dextral Pb element in *A. viirae* sp. nov. has a wavy edge (in lateral view, Fig. 4q), while in *A. superbus* it is straight with distal ends of the process pointing upwards (Fig. 5r) or downwards (Fig. 5s). The denticles on posterior and anterior processes on both Pb elements of *A. superbus* are more prominent (Fig. 5r, t) compared with the denticulation on Pb element of *A. viirae* sp. nov. (Fig. 4q, w). Additionally, the cusps of the sinistral Pb (Fig. 5t) and dextral Pb elements (Fig. 5s) of *A. superbus* are of similar size, but in *A. viirae* sp. nov. the cusp of the sinistral Pb (Fig. 4w) is half the size of that of the dextral Pb element (Fig. 4t). The processes of the S elements in *A. viirae* sp. nov. (Fig. 4al) are more densely denticulated and denticles laterally compressed to a higher degree than in *A. superbus* (Fig. 5aa). The strongly backwards-turned posterior denticle characteristic of the M element of *A. viirae* sp. nov. (Fig. 4z, aa, ac, ah, ai) is missing in *A. superbus* (Fig. 5j) or only occurs as a small barb-like tooth (Fig. 5i). Additionally, the number of anteriorly directed denticles including an often undistinguishable cusp on the anterior end of the M element vary noticeably in *A. viirae* sp. nov. (Fig. 4y–ac), whereas the element of *A. superbus* has only two anteriorly directed denticles a cusp and an additional denticle (Fig. 5i–l).

Remarks. One dextral Pa element (Fig. 5a) and some probable M elements (Fig. 5b–e) of *A. viirae* sp. nov. were found together with typical dextral Pa and M elements of *A. tvaerensis* (Fig. 5f and Fig. 5g, h, respectively) in the interval 318.5–318.6 m, well below the last occurrence of *A. tvaerenis* at 316.4 m. The continuous range of *A. viirae* sp. nov. starts at 316.55 m. Because such an earlier occurrence of *A. viirae* sp. nov. in a single sample below the interval of continuous range of this taxon has not been recorded in the Ruhnu and Velise core sections (restudy of collections published by Männik, 2003 and Paiste *et al.* 2022, respectively), this is currently considered to be as a result of contamination. Further studies of other sections are required to determine the actual situation.

From the *B. gerdae* and *B. alobatus* CSzs in the Tartu core section, from the interval coeval with that yielding *A. viirae* sp. nov. in the Mehikoorma core section, *Amorphognathus* cf. *tvaerensis*,

Amorphognathus n. sp. and *Amorphognathus* sp. A were identified by Stouge (1998). However, as no description and illustrations of these taxa were provided, it is not possible to confirm whether (some of) these conodonts might belong to *A. viirae* sp. nov.

The variation in morphology of P and M elements of *A. tvaerensis* has been noticed by many authors (Dzik, 1990, 1994; Stouge, 1998; Viira, 2008; Xu *et al.* 2010; Paiste *et al.* 2022). The first illustrations of the elements described here as *A. viirae* sp. nov. come from the Äiamaa, Are and Ohesaare core sections in Estonia (Viira, 1974). No additional description or information was provided. The first reference outside Estonia is from the Mójcza section in Poland. From this section, Dzik (1990, figs 17, 18, depth *c.* 2 m) illustrated the evolution of *Amorphognathus* in the Mójcza section with figures of transitional Pa elements between *A. tvaerensis* and *A. superbus*. These elements lack the small lateral lobe anterior of the extra postero-lateral process, noticeable shortening of the extra postero-lateral process and elongation of the anterior branch on inner lateral process. An additional illustration of the evolution of *Amorphognathus* in the same section by Dzik (1999b, fig. 5) shows a dextral Pa element that is more similar to *A. viirae* sp. nov. In a more detailed description of the Mójcza section, Dzik (1994) shows a general outline of a fragmented dextral Pa element (Dzik, 1994, fig. 22: sample 93), describing this element as an early form of *A. superbus*, morphologically transitional between the typical representatives of *A. tvaerensis* and *A. superbus*. However, later transitional elements were reidentified as *A.* aff. *ventilatus* (Dzik, 1999a). Additional samples from the Mójcza section yielded elements that were designated as *A.* aff. *ventilatus* or assigned as late forms of *A. tvaerensis* (Dzik, 1999a, pl. 1, figs 22–26). The illustrations of the Pa elements of *A. viirae* sp. nov. from the Mójcza section are morphologically more variable than those from the Mehikoorma section. The lateral lobe of posterior process of the dextral Pa elements in the Mehikoorma section is rarely denticulated (Fig. 4b, e), but this feature is very common on elements from the Mójcza section (Dzik, 1994, text-fig. 22: 93, 96; Dzik, 1999a, pl. 1, figs 1–26).

The strata in the Mehikoorma section containing *A. viirae* sp. nov. are overlain by an interval of depth almost 13 m (310.6–297.75 m) yielding no specimens of *Amorphognathus*. For that reason, the full range of *A. viirae* sp. nov. and its relationship to the younger representatives of *Amorphognathus* cannot be identified precisely; however, it is evident that *A. tvaerensis* is the ancestor of *A. viirae* sp. nov. and *A. superbus* is its descendant. This conclusion is supported by data from the stratotype section of the base of the Katian Stage (Black Knob Ridge Section; Goldman *et al.* 2007). The uppermost illustrated Pa elements of *A. tvaerensis* from the Black Knob Ridge Section, 4.3 m below the lower boundary of the Katian Stage (Goldman *et al.* 2007, fig. 7: 17, 18), are similar to those of *A. viirae* sp. nov. and, before direct study of these specimens, can be tentatively considered as conspecific. Most noticeably, the dextral Pa element (Goldman *et al.* 2007, fig. 7: 18) from the Black Knob Ridge Section lacks the small lateral lobe anterior to the extra postero-lateral process inherent to *A. tvaerensis* (Ferretti & Bergström, 2022, fig. 4a–h), and the anterior branch on the inner lateral process is as long as the anterior process, similar to that of *A. viirae* sp. nov. elements (Fig. 4a). Other illustrated Pa elements of *Amorphognathus* from the Black Knob Ridge Section, from 1.7 m above the Katian boundary, were originally identified as *Amorphognathus* sp. with probable affiliation to *A. superbus* (Goldman *et al.* 2007, fig. 7:15, 16). These illustrated specimens resemble elements of typical *A. superbus*, suggesting that *A. superbus* might really be a successor of *A. viirae* sp. nov. However, as in the Black Knob Ridge Section, ranges of *A. viirae* sp. nov. and

A. superbus are separated by an unsampled interval of thickness *c.* 5 m and the morphological changes in transition between *A. viirae* sp. nov. and *A. superbus* are currently not observed.

The reinvestigation of formerly published conodont collections from the Swedish sections carried out by TP with the kind permission of S. Bergström confirmed that collections from the Fjäcka main section and the Smedsby Gård drillcore (distribution of taxa characterized in Bergström, 2007 and Bergström *et al.* 2011, respectively, but specimens not illustrated), contain *A. viirae* sp. nov.

Only one M element of *A. viirae* sp. nov., with distinctive curved posteriorly directed denticle, was found in the Smedsby Gård drillcore at depth 93.04–93.10 m. The upper part of the previously described range of *A. tvaerensis* contains mostly elements determinable as *Amorphognathus* sp. only. In the Fjäcka main section *A. viirae* sp. nov. was identified at depth 15.05–17.30 m (according to sample labels), above the base of the Dalby Limestone, where recognizable fragments of the dextral Pa elements occur. A single M element in this section also comes from the sample 15.05 m above the base of the Dalby Limestone. It is noteworthy that between the uppermost identifiable *A. tvaerensis* (13.05–13.10 m above the base of Dalby Limestone) and the lowermost *A. viirae* sp. nov. sample (15.05–15.10 m above the base of Dalby Limestone) there is a 1.95 m interval with samples that yielded only rare and poorly preserved elements that could be identified only as *Amorphognathus* sp.

Material. Mehikoorma section: 31 dextral Pa, 25 sinistral Pa, 14 dextral Pb, 14 sinistral Pb, 90 M and about 100 S elements; Velise section: 10 dextral Pa, 8 sinistral Pa, 7 dextral Pb, 10 sinistral Pb, 13 M and about 50 S elements; Ruhnu section: 5 dextral Pa, 4 sinistral Pa, 4 dextral Pb, 5 sinistral Pb, 10 M and about 40 S elements; Fjäcka Main section: 5 dextral Pa, 1 sinistral Pa, 1 M and about 50 Pb and S elements; Smedsby Gård drillcore: 1 M element.

Distribution. In all sections where A. *viirae* sp. nov. can be identified, the first appearance datum (FAD) of the species falls within the upper range of *B. gerdae* or within the lowermost range of *B. alobatus* (when *B. gerdae* is absent or when *Amorphognathus* can only be identified on genus level within *B. gerdae* range). Baltoscandian region: upper half of the Sandbian; Abja section: Adze Formation (429.3 m); Äiamaa section: Tatruse Formation (196.08 m); Are section: Tatruse Formation (291.7 m); Fjäcka Main section: Dalby limestone (15.05–17.85 m above the base). Holy Cross Mountains: Mójcza Quarry, Mójcza limestone (samples 93–97 in Dzik, 1994, text-fig. 22); Mehikoorma section: Tatruse and Kahula formations (310.6–316.2 m); Ohesaare section: Tatruse Formation (473.8–471.8 m); Ruhnu section: Adze Formation (656.8–653.8 m); Smedsby Gård drillcore: Dalby limestone (93.04–93.10 m); Velise section: Tatruse and Kahula formations (202.54–197.74 m).

Amorphognathus superbus (Rhodes, 1953)

1953 *Holodontus superbus* sp. nov.; Rhodes (1953, p. 304, pl. 21: 125–127).

1964 *Holodontus superbus* Rhodes (1953); Bergström (1964, p. 26–7, text-fig. 11).

1971 *Amorphognathus superbus* Rhodes (1953); Bergström (1974, pl. 2: 8, 9).

1976 *Amorphognathus superbus* Rhodes (1953); Dzik (1976, fig. 28a–e, ?f–i).

?1980 *Amorphognathus superbus* Rhodes (1953); Merrill (1980: fig. 5: 9, 10, not including fig. 4:1).

1980 *Amorphognathus complicatus* Rhodes (1953); Merrill (1980, fig. 4:10 not including 2–9, 11–23).

Fig. 5. *Amorphognathus* in the Mehikoorma core section. (a–e) *Amorphognathus viirae* sp. nov.: (a) dextral Pa element, posterior process, upper view, sample 318.5–318.6 m, specimen GIT870-57; (b) dextral M element, lateral view, sample 318.5–318.6 m, specimen GIT870-439; (c) sinistral M element, lateral view, sample 318.5–318.6 m, specimen GIT870-434; (d) sinistral M element, lateral view, sample 318.5–318.6 m, specimen GIT870-435; (e) dextral M element, lateral view, sample 318.5–318.6 m, specimen GIT870-437. (f–h) *Amorphognathus tvaerensis* (Bergström, 1962): (f) dextral Pa element, upper view, sample 318.5–318.6 m, specimen GIT870-55; (g) sinistral M element, lateral view, sample 318.5–318.6 m, specimen GIT870-446; (h) sinistral M element, lateral view, sample 318.5–318.6 m, specimen GIT870-447. (i–am) *Amorphognathus superbus* (Rhodes, 1953): (i) sinistral M element, lateral view, sample 294.7–294.8 m, specimen GIT870-573; (j) dextral M element, lateral view, sample 288.2–288.3 m, specimen GIT870-613; (k) sinistral M element, lateral view, sample 290.1–290.2 m, specimen GIT870-595; (l) dextral M element, lateral view, sample 292.8–292.9 m, specimen GIT870-577; (m) dextral Pa element, posterior process, upper view, sample 290.1–290.2 m, specimen GIT870-196; (n) sinistral Pa element, posterior process, upper view, sample 289.7–289.8 m, specimen GIT870-209; (o) probable fragment of sinistral Pa element, posterior process, upper view, sample 296.3–296.4 m, specimen GIT870-149; (p) dextral M element, lateral view, sample 296.3–296.4 m, specimen GIT870-570; (q) dextral Pb element, upper view, sample 290.1–290.2 m, specimen GIT870-348; (r) dextral Pb element, inner-lateral view, sample 290.7–290.8 m, specimen GIT870-342; (s) dextral Pb element, inner-lateral view, sample 291.2–291.3 m, specimen GIT870-338; (t) sinistral Pb element, outer-lateral view, sample 292.2–292.3 m, specimen GIT870-330; (u) sinistral Pb element, upper view, sample 290.1–290.2 m, specimen GIT870-346; (v) sinistral Pb element, upper view, sample 291.2–291.3 m, specimen GIT870-335; (w) Sa element, lateral view, sample 290.7–290.8 m, specimen GIT870-790; (x) Sd element, lateral view, sample 292.8–292.9 m, specimen GIT870-765; (y) Sb element, lateral view, sample 292.8–292.9 m, specimen GIT870-766; (z) Sd element, lateral view, sample 290.1–290.2 m, specimen GIT870-803; (aa) Sd element, lateral view, sample 295.8–295.9 m, specimen GIT870-741; (ab) Sd element, lateral view, sample 292.8–292.9 m, specimen GIT870-767; (ac) Sb element, lateral view, sample 290.7–290.8 m, specimen GIT870-793; (ad) Sc element, lateral view, sample 290.1–290.2 m, specimen GIT870-809; (ae) Sc element, lateral view, sample 290.1–290.2 m, specimen GIT870-810; (af) Sc element, lateral view, sample 294.7–294.8 m, specimen GIT870-755; (ag) Sc element, lateral view, sample 292.8–292.9 m, specimen GIT870-768; (ah) sinistral M element, lateral view, sample 295.8–295.9 m, specimen GIT870-571; (ai) sinistral M element, lateral view, sample 291.9–292 m, specimen GIT870-586; (aj) dextral M element, lateral view, sample 291.2–291.3 m, specimen GIT870-590; (ak) sinistral M element, lateral view, sample 290.1–290.2 m, specimen GIT870-594; (al) sinistral M element, lateral view, sample 289.3–289.4 m, specimen GIT870-607; (am) sinistral M element, lateral view, sample 289.3–289.4 m, specimen GIT870-608. (an–at) *Amorphognathus ventilatus* (Ferretti & Barnes, 1997): (an) sinistral M element, lateral view, sample 292.8–292.9 m, specimen GIT870-580; (ao) dextral M element, lateral view, sample 292.8–292.9 m, specimen GIT870-581; (ap) dextral M element, lateral view, sample 292.8–292.9 m, specimen GIT870-582; (aq) sinistral M element, lateral view, sample 292.2–292.3 m, specimen GIT870-583; (ar) sinistral M element, lateral view, sample 292.2–292.3 m, specimen GIT870-584; (as) sinistral M element, lateral view, sample 292.2–292.3 m, specimen GIT870-585; (at) dextral M element, lateral view, sample 291.9–292 m, specimen GIT870-587. (au–az) *Amorphognathus complicatus* (Rhodes, 1953): (au) probable fragment of dextral Pa element, posterior process, upper view, sample 288.2–288.3 m, specimen GIT870-229; (av) sinistral Pa element, upper view, sample 288.6–288.7 m, specimen GIT870-223; (aw) sinistral M element, lateral view, sample 288.6–288.7 m, specimen GIT870-609; (ax) dextral M element, lateral view, sample 288.6–288.7 m, specimen GIT870-610; (ay) sinistral M element, lateral view, sample 288.2–288.3 m, specimen GIT870-614; (az) sinistral M element, lateral view, sample 289.7–289.8 m, specimen GIT870-605. All scale bars are 100 μm.

1980 *Amorphognathus superbus* Rhodes (1953); Orchard (1980, 16, 17, pl. 4: 19, 20, 24).

1985 *Amorphognathus superbus* Rhodes (1953); Savage and Bassett (1985, p. 692, 694, pl. 83: 1–19).

1994 *Amorphognathus superbus* Rhodes (1953); Dzik (1994, p. 93–94, text-fig. 22: samples 100–112; not including pl. 23: 3–5).

1999a *Amorphognathus superbus* Rhodes (1953); Dzik (1999a, p. 246, pl. 1: 27–30).

2007 *Amorphognathus* sp.; Goldman *et al.* (2007, fig. 7: 15, 16).

2014a *Amorphognathus superbus* Rhodes (1953); Ferretti *et al.* (2014a, p. 819–21, fig. 12Z, AA).

2014b *Amorphognathus superbus* Rhodes (1953); Ferretti *et al.* (2014b, p. 114–6, pl. 1: 13–15).

2017 *Amorphognathus superbus* Rhodes (1953); Männik (2017, fig. 4M, R, S, U, ?P).

Diagnosis. Rhodes (1953, p. 304).

Remarks. The type specimen of *A. superbus* is a poorly preserved M element (Rhodes, 1953, pl. 21, figs 125–127), refigured by Bergström (1964, text-fig. 11). The holotype has a central cusp with two smaller denticles on both sides of it, the larger (roughly half the size of the cusp) on the anterior process and a tiny denticle on the posterior side. Only the posterior process of the holotype is denticulated. The M element illustrated by Bergström (1971, pl. 2, fig. 9) in the multi-element description of *A. superbus* seems to have a discrete denticle on all processes. The dextral Pa element of *A. superbus* can be distinguished from those of *A. tvaerensis* by lack of an 'extra' postero-lateral process on its outer side (Bergström, 1971).

The M element from the Mehikoorma section, interval 294.7–294.8 m (Fig. 5i), is similar to the holotype of *A. superbus* in having a central cusp with two smaller denticles on both sides of it, the larger on the anterior process and a smaller, barb-like denticle on the posterior side. Only the posterior process of the specimen is denticulated. Elements of similar morphology occur up to the uppermost studied sample in the section (288.2–288.3 m; Fig. 5j) and both types of specimens, with (Fig. 5i, k) and without (Fig. 5j, l) the barb-like denticle, are present. No complete Pa element of *A. superbus* was found, and only a few larger fragments of it could be assigned to this species (Fig. 5m, n). The lowermost of such elements comes from the sample 296.3–296.4 m (Fig. 5o) where it occurs together with an M element of morphology characteristic of *A. superbus* (Fig. 5p).

Variation in morphology of *A. superbus* elements in the Mehikoorma section is difficult to address as no complete Pa were found, and Pb (Fig. 5q–v) and S (Fig. 5w–ag) elements are too poorly preserved. The 'strongly sinuous aboral inner margin' (Savage & Bassett, 1985, p. 692) considered to be characteristic of the sinistral Pb element of the *A. superbus* was not recognized in sinistral Pb elements from the studied samples. The M elements that are morphologically similar to those of *A. superbus*, but have a denticulated anterior process (Fig. 5p, ah–ak) or a prominent barb-like denticle on their posterior processes (Fig. 5al, am), are considered here as varieties of the M elements of *A. superbus*. This conclusion is based on the fact that at the time of wide morphological variation of M elements (Fig. 5i–l, p, ah–am; online Supplementary Fig. S13e, g, i, j, s, t, v–x, aa–ai, ap, aq) no distinct changes in morphology of other elements were observed (Fig. 5m–o, q–ag; online Supplementary Figs S4ad–an, S5a–aw, S6a–ah, S8n–bi, S15ah–br, S16a–bv, S17a–q). Several M elements earlier identified as *Amorphognathus* sp. (aff. *A. duftonus* Rhodes) by Männik (2017, fig. 4M, R, S, U) are evidently elements of *A. superbus* as understood here.

Material. Mehikoorma section: 6 dextral Pa, 2 sinistral Pa, 15 dextral Pb, 14 sinistral Pb, 23 M and about 200 S elements; Velise section: 2 dextral Pa, 1 sinistral Pa, 1 dextral Pb, 2 sinistral Pb and 4 S elements; Ruhnu section: 4 dextral Pa, 3 sinistral Pa, 7 dextral Pb, 9 sinistral Pb, 3 M and about 20 S elements; Fjäcka Main section: 1 M.

Distribution. The first M element of the *A. superbus* that is similar to the element shown in Figure 5i was recovered 4.9–5.0 m above the base of the Skagen Formation in the Fjäcka main section, determined by TP. As demonstrated by Goldman *et al.* (2007, see also remarks to *A. viirae* sp. nov.), the FAD of *A. superbus* is located at or near the lower boundary of the Katian Stage in the boundary stratotype section. Balto-scandian region: lower half of the Katian Stage; Mehikoorma section: Variku Formation (288.2–296.4 m in the studied part of the section, Fig. 2); Ruhnu section: Mossen and Mõntu formations (645–633 m); Velise section: Hirmuse and Rägavere formations (176.75–173.0 m); Fjäcka Main section: 4.9–5.0 m above the base of the Skagen Formation.

Amorphognathus ventilatus (Ferretti & Barnes, 1997)

1974 *Holodontus* sp. nov.; Viira (1974, p. 90, fig. 110).

1997 *Amorphognathus ventilatus* sp. nov.; Ferretti & Barnes (1997, p. 28–29, pl. 2: 14–17).

2014a *Amorphognathus ventilatus* Ferretti & Barnes (1997); Ferretti *et al.* (2014a, p. 821–3, figs 7V, 12S–U).

2014b *Amorphognathus ventilatus* Ferretti & Barnes (1997); Ferretti *et al.* (2014b, p. 116, pl. 1: 17, 18).

Diagnosis. Ferretti & Barnes (1997, p. 28–9).

Remarks. Originally, *A. ventilatus* was established based on the morphology of its M element from the *A. ordovicicus* CZ from Kalkbank limestone, Schmiedefeld area, Thuringia, Germany (Ferretti & Barnes, 1997). In the remarks to their new species, Ferretti & Barnes (1997) referred to the specimen from the Ohesaare core section illustrated by Viira (1974, fig. 110, depth 461.95 m, *A. superbus* CZ) as a probable element of *A. ventilatus*. Additional M elements identified as *A. ventilatus* were also recognized by Ferretti *et al.* (2014a, Whitland A40 road cut, Wales, *A. ordovicicus* CZ; 2014b, Portrane Limestone at Portrane, Ireland, *A. ordovicicus* CZ). Only the M element of *A. ventilatus* is currently known.

In the Mehikoorma section, probable M elements of *A. ventilatus*, morphologically similar to those described and figured by Viira (1974, fig. 110), occur together with *A. superbus* in the interval 292.9–291.9 m (Figs 2, 5an–at). No P or S elements that could be distinguished from those of *A. superbus* were found. It is currently unclear whether *A. ventilatus* recognized in Estonian sections is conspecific with that described by Ferretti & Barnes (1997). Estonian specimens come from an older interval (the *A. superbus* CZ) than the type material that is described from the *A. ordovicicus* CZ. Furthermore, there is no indication of probable P or S elements of *A. ventilates*, raising the question of whether the M elements in Estonian material assigned to *A. ventilatus* may simply represent a variety of *A. superbus*.

Material. Mehikoorma section. 7 specimens.

Distribution. Estonia: lower half of the Katian Stage; Mehikoorma section: Variku Formation (292.9–291.9 m, Fig. 2); Ohesaare section: Paekna Formaiton (461.95 m).

Amorphognathus complicatus (Rhodes, 1953)

1953 *Amorphognathus complicatus* sp. nov.; Rhodes (1953, p. 282, pl. 20: 42, 45, 46).

?1966 *Amorphognathus complicata* Rhodes (1953); Hamar (1966, p. 53, pl. 7:2–4).

Fig. 6. Relationships between the Sandbian and Katian boundaries with conodont zones within Atlantic Realm Conodont Zone successions (Nõlvak *et al.* 2006; Bergström *et al.* 2007; Männik *et al.* 2021). Mid. – Middle; Dar. – Darriwilian; Kat. – Katian.
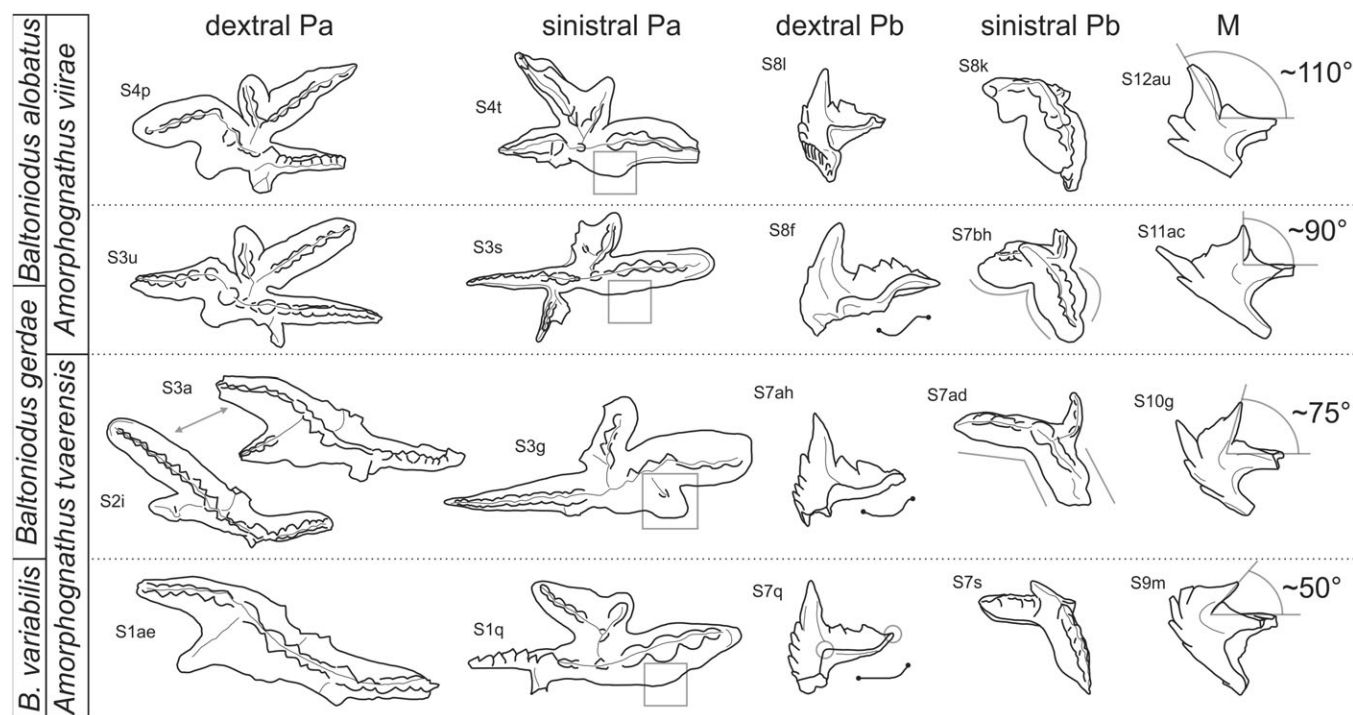

Fig. 7. Variations of *A. tvaerensis* and *A. viirae* sp. nov. elements in Mehikoorma section within the distribution interval of *Baltoniodus variabilis*, *B. gerdae* and *B. alobatus*. Elements are not to scale. Numbers with letters next to elements refer to the illustrations in the Supplementary Material. Double-headed arrow points to the posterior process of dextral Pa element. Square marks the lateral extension on the outer side of the posterior process on sinistral Pa elements. Circles indicate ends of the inner edge of posterior process of dextral Pb elements, and the line below the figure repeats the shape of the edge in lateral view.

?1980 *Amorphognathus superbus* Rhodes (1953); Merrill (1980, fig. 4:1, not including fig. 5: 9, 10).

1980 *Amorphognathus complicatus* Rhodes (1953); Merrill (1980, fig. 4:2–9, 11–23, not including 10).

1980 *Amorphognathus* aff. *complicatus* Rhodes (1953); Orchard (1980, p. 16, pl. 6: 30).

2017 *Amorphognathus complicatus* Rhodes (1953); Männik (2017, figs 4Q, 5A).

Remarks. Both Pa elements were illustrated by Rhodes (1953). They are characterized, additionally to anterior and posterior processes, by a smaller bifurcated outer lateral process next to the cusp and an inner posterolateral process of almost equal size to the posterior process. The simple, unbranched inner lateral process is the main feature allowing the Pa elements of *A. complicatus* to be separated from those of *A. ordovicicus* (Rhodes, 1953). The S elements of *A. complicatus* are figured by Merrill (1980) and are generally

similar to those of other representatives of the genus *Amorphognathus*. The sinistral Pa element illustrated by Merrill (1980, fig. 4:10) possesses an inner lateral process with two branches. This suggests that it most probably does not belong to *A. complicatus* but instead to *A. superbus*. Another sinistral Pa element described as *A. superbus* (Merrill, 1980, fig. 4:1) probably does belong to *A. complicatus* as the inner lateral process is unbranched. The M element of *A. complicatus* (Merrill, 1980, fig. 4:22) has a prominent proclined cusp with a single smaller anterior denticle. The posterior and inner lateral processes bear a single denticle in their distal parts. The main difference between the M elements of *A. complicatus* and *A. superbus* is that the cusp of the element in the former taxon is considerably larger (taller) in comparison to the denticle located just anterior of it (Fig. 5aw, ax) and to that of *A. superbus* (Fig. 5k). The Pa elements of *A. complicatus* have characteristic wide basal platforms (Rhodes, 1953, pl. 20, fig. 42; Merrill 1980, fig. 4:3; Orchard 1980, pl. 6, fig. 30; Männik 2017, fig. 4Q). Denticles on the processes are connected by ridges (Fig. 5av). In some cases, the denticles may also be elongated perpendicularly to the main axis of the process (sometimes so strongly that there seems to be two denticles instead of one) and bear sharp ridges oriented in the same direction (Fig. 5au). Apices on the processes are not very sharply pointed. It is currently unclear if the complex denticle morphology is characteristic of *A. complicatus* or shared with other species of similar age. Furthermore, Pb and S elements of *A. complicatus* are indistinguishable from those of *A. superbus* apparatus within studied sections.

In the Mehikoorma core section, *A. complicatus* has been found in the three samples studied from the interval 288.2–289.4.7 m (Fig. 2), where it co-occurs together with *A. superbus*.

Material. Mehikoorma section: 1 sinistral Pa, 5 M; Velise section: 1 dextral Pa; Ruhnu section: 2 dextral Pa, 8 M.

Distribution. Estonia: lower–middle parts of the Katian Stage; Mehikoorma section: Variku Formation (288.2–288.7 m in the studied part of the section, Fig. 2); Ruhnu section: Mossen and Mõntu formations (640.5–635 m); Velise section: Rägavere Formation (173.0–173.07 m).

5. Discussion

5.a. Concluding taxonomic remarks

Morphologically distinct *A. inaequalis* has been reported and illustrated only from the sections of Wales and France (Ferretti & Bergström, 2022). However, a subzone established based on this species is also included in regional conodont zonation in Sweden (Bergström, 2007) and Estonia (Meidla *et al.* 2014). A re-study of collections from the Fjäcka (Bergström, 2007) and Smedsby Gård (Bergström *et al.* 2011) sections from Sweden, and from the Ruhnu (Männik, 2003) and Mehikoorma (Männik & Viira, 2005) core sections from Estonia, from where *A. inaequalis* was reported earlier, revealed that all these identifications are highly problematic; most probably, all specimens identified as *A. inaequalis* actually belong to *A. tvaerensis*.

The morphological variation of elements of *A. tvaerensis* in its upper range has been discussed by several authors. Specimens from this interval have been assigned to an early form of *A. superbus* (Dzik, 1994), to *A.* aff. *ventilatus* or to a late form of *A. tvaerensis* (Dzik, 1999a), and to *A.* cf. *tvaerensis*, *Amorphognathus* n. sp. or *Amorphognathus* sp. A. (Stouge, 1998). The present study of rich material from the Mehikoorma core section demonstrates that, in the interval starting from the uppermost *B. gerdae* CSz up to the

level of temporal disappearance of *Amorphognathus* in the section in the *B. alobatus* CsZ, a distinct species of *Amorphognathus* exists, morphologically different from *A. tvaerensis* and described above as *Amorphognathus viirae* sp. nov. Its most distinct, dextral Pa element is characterized by a sinuous curvature of the main blade, an occurrence of a distinct lateral lobe on the outer side of the posterior process and bifurcated lateral processes on both sides of the element. The M element of *A. viirae* sp. nov. has a prominent, posterior denticle, the distal part of which is curved anteriorly. This new species has so far been found in Estonian and Swedish sections, with probable occurence also in Polish (Holy Cross Mountains) and Oklahoma (Black Knob Ridge) sections based on published figures.

The high morphological variation of the M element in *A. tvaerensis* (online Supplementary Figs S9a–az; S10a–s, ab–bb; S11a–s), *A. viirae* sp. nov. (online Supplementary Figs S10t–aa; S11t–ba; S12a–av) and *A. superbus* (online Supplementary Fig. S13a, b, d–j, q, s–ai, al, am, ap–ar) indicates that definition/identification of species in the *Amorphognathus* lineage based only on this element might be highly problemtic.

5.b. Biostratigraphical considerations

The absence of *A. inaequalis* and presence of *A. viirae* sp. nov. within Estonian and Swedish sections necessitates a revision of the conodont zonations of Baltoscandia. The concept of the *A. tvaerensis* CZ and its subzones, based on the succession of species of the *Baltoniodus* lineage and with the lower boundary drawn at the appearance level of *A. inaequalis*, would be difficult to maintain in the situation where the formerly identified specimens of *A. inaequalis* in Estonia and Sweden are attributed to *A. tvaerensis* and the specimens in the upper part of the range of *A. tvaerensis* are assigned to the new species, *A. viirae* sp. nov. While the former *B. gerdae* CSz and *B. alobatus* CSz are easily recognizable and seemingly reliable, the appearance of *B. variabilis* is reported as a gradual transition from its predecessor *B. prevariabilis* (e.g. Dzik, 1978). The *prevariabilis–variabilis* transition has not been examined in detail in the Baltoscandian sections, but the appearance of *B. variabilis* may be the best approximation of the lower boundary of the Sandbian (and Upper Ordovician) strata in the conodont succession. This boundary is currently drawn within the *Pygodus anserinus* CZ, and the appearance of *B. variabilis* is documented from the first samples above the lower boundary of the Sandbian Stage in its stratotype section (Bergström *et al.* 2000). Further careful investigation of the morhpological transition between *B. prevariabilis* and *B. variabilis* is essential for clarifying the potential of *B. variabilis* as a possible marker of the lower boundary of Sandbian Stage in the Baltoscandian conodont succession. The fact that the Fågelsång Phosphate in the Sandbian stratotype section is considered to mark a sedimentary cap in the succession (Goldman *et al.* 2020) would make the use of *A. tvaerensis* CZ as the marker of lower boundary of the Sandbian Stage rather arbitrary. In several sections of Argentina the appearance of *B. variabilis* coincides with the appearance of *Nemagrapthus gracilis*, but again right above a hiatus in the succession (Serra *et al.* 2015; Feltes *et al.* 2018).

As there is no *A. inaequalis* in the sections of Estonia and Sweden, it would be reasonable to abandon the previous *A. inaequalis* CZ (Viira, 2008) or *A. inaequalis* CSz (Bergström, 2007; Meidla *et al.* 2014). The last recorded elements of genus *Pygodus* in the Velise and Mehikoorma sections are succeeded upsection by the first appeerance of *Amorphognathus*. An overlap

between the ranges of *P. anserinus* and *A. tvaerensis* is recorded from the Smedsby Gård (Bergström *et al.* 2011), Kovel-1 (Saadre *et al.* 2004) and Bliudziai-150 (Stouge *et al.* 2016) sections. A small gap between the ranges is present in Fjäcka (Bergström, 2007), Ruhnu (Männik, 2003) and Viki (Männik, 2010; Hints *et al.* 2014) sections, probably because of poor yield and/or poor preservation of conodonts. In the sections without a notable hiatus, the base of the *A. tvaerensis* CZ is located within the upper range of *P. anserinus*.

A transition between *A. viirae* sp. nov. and *A. superbus* is not documented in the Ordovician succession of Baltoscandia because of a scarcity of *Amorphognathus* in the Sandbian–Katian boundary interval. This barren interval, poorly represented by specimens of this genus, has been documented in all known sections in the region from Sweden, Estonia, Latvia and Poland. Previously, this interval had been considered to correspond to the Mid-Caradoc Event (Männik, 2003, 2004; Männik & Viira, 2005), with noticeable changes in conodont succession occurring along with an episode of biotic, climatic, sea-level and facies changes.

It is possible that *A. tvaerensis* reported earlier from the stratotype section of the Katian Stage (Goldman *et al.* 2007) and from Argentina (Ortega *et al.* 2008) also includes *A. viirae* sp. nov. The lowermost elements of *Amorphognathus* in the Katian stratotype (Goldman *et al.* 2007, fig. 7:15, 16), somewhat above the base of the Katian Stage, are identified as *Amorphognathus* sp. cf. *A. superbus*. The figured *A. tvaerensis* from this section (Goldman *et al.* 2007, fig. 7:17–22) is similar to *A. viirae* sp. nov., as discussed here in Section 4 (Systematic description). Additionally, a high-resolution conodont–graptolite study from Argentina (Ortega *et al.* 2008) revealed a conodont succession simlar to that in the boundary interval of type section of the Katian Stage. The uppermost *A. tvaerensis* in the La Invernada Range (probably *A. viirae* sp. nov. based on information from Batloscandian and Katian stratotype successions) occurs below the FAD of *D. caudatus* in the section and therefore also below the base of the Katian Stage (Ortega *et al.* 2008, fig. 2). It is noteworthy that the latest *B. alobatus* disappears at the same level and the appearance of *A. superbus* is recorded above the FAD of *D. caudatus*.

Considering the data above, we propose an updated conodont zonation for the Sandbian – lower Katian interval (Fig. 6) that probably has the potential to be applied all over the Atlantic Realm in the sense of Pyle & Barnes (2002). The former subzone of the *A. tvaerensis* CZ, *A. inaequalis* CsZ, is removed from the scheme because, according to current knowledge, *A. inaequalis* has a very limited geographical distribution; it has only been reliably identified from Wales and France (Ferretti & Bergström, 2022). The former *B. variabilis*, *B. gerdae* and *B. alobatus* subzones of the *A. tvaerensis* CZ are treated here as CZs. The *A. tvaerensis* CZ is redefined and, as a new one, the *A. viirae* CZ is included in the scheme. Lower boundaries of all zones in the revised version of the scheme correspond to the FADs of the nominate taxa (Fig. 6). The last appearance datum (LAD) of *B. alobatus* and the FAD of *A. superbus* are separated by an interval that does not yield biostratigraphically diagnostic conodonts. In the proposed scheme this interval is tentatively included in the *B. alobatus* CZ. The Sandbian–Katian boundary lies in the upper part of this interval.

The morphological variation of the elements of *A. tvaerensis* and *A. viirae* sp. nov. in the succession may offer some clues for a more detailed stratigraphic subdivision (Fig. 7). The P and M elements of *A. tvaerensis* show a noticeable variation in the *B. gerdae* CZ. Typically, posterior process of the dextral Pa element of *A. tvaerensis* is curved (Fig. 7:S1ae, S3a). However, in the *B. gerdae*

CZ elements with a straight posterior process are also present (Fig. 7, double-headed arrow pointing to S2i). Additionally, a sinistral Pa element of *A. tvaerensis* in the *B. gerdae* CZ possesses a distinct lateral lobe on the outer side of its posterior process (Fig. 7, square on the S3g) which is missing on the elements below this level, in the *B. variabilis* CZ (Fig. 7, square on S1q). Furthermore, the dextral Pb element of *A. tvaerensis* has, in lateral view, a slightly undulating inner edge of posterior process in the *B. variabilis* CZ (Fig. 7:S7q, indicated by a circles and line below the figure), it becomes more evident on elements from the upper part of *A. tvaerensis* range in the *B. gerdae* CZ (Fig. 7:S7ah) and is particularly distinct on, and characteristic of, elements in *A. viirae* sp. nov. (Fig. 7:S8f). In the *B. gerdae* CZ, the angle between the posterior process and the posterior denticle of the M elements of *A. tvaerensis* increases from *c.* 50° (Fig. 7:S9m) in the lower part of the CZ to 75° (Fig. 7:S10g) in the upper part. The P and M elements of *A. viirae* also changed in time. Most noticeably, the angle between the posterior process and posterior denticle of the M elements increases from *c.* 90° (Fig. 7:S11ac) to 110° (Fig. 7:S12au). Most of the sinistral Pa elements in the upper part of the *A. viirae* sp. nov. range have a poorly developed lateral extension on the outer side of the posterior process (Fig. 7, square on S4t), a feature missing from elements of the lower range interval of the species (Fig. 7, square on S3s). Additionally, the shape of the outer edge of the process of the sinistral Pb elements become more laterally expanded within the upper range of *A. viirae* sp. nov. (Fig. 7: S8k), a trend of gradual morphological change from elements of *A. tvaerensis* (Fig. 7:S7ad) to those of *A. viirae* sp. nov. (Fig. 7:S7bh).

6. Conclusions

The re-study of rich collections of Sandbian – lower Katian conodonts from Estonia (Mehikoorma and Ruhnu core section) and Sweden (Fjäcka and Smedsby Gård sections) revealed that *A. inaequalis* is missing in this part of the Baltoscandian region. However, the probable occurrence of this species has been reported from Lithuania (Bliudziai-150 core section) but also from Ukraine (Kovel-1 core section). Further studies are required to prove the occurrence of *A. inaequalis* in these regions.

The re-study of *A. tvaerensis* revealed that the specimens of *Amorphognathus*, previously considered to belong to the younger representatives of this taxon, are actually morphologically quite different. Here, they are described as a new species: *Amorphognathus viirae* sp. nov. To date, outside Estonia the new species has been recognized in some sections in Sweden (re-study of collections by TP). Based on an analysis of published figures, it also evidently occurs in Poland (Mójcza Quarry, Holy Cross Mountains) and the USA (Black Knob Ridge, Oklahoma).

The absence of *A. inaequalis* in the Baltoscandian conodont succession and recognition of the new species *A. viirae* sp. nov. resulted in the revision of the Sandbian stratigraphic scheme in the region. The zonation proposed here yields (from below) the *P. anserinus*, *B. variabilis*, *A. tvaerensis*, *B. gerdae*, *A. viirae* and *B. alobatus* CZs.

to personally thank S. M. Bergström for providing the opportunity to study conodont samples from Swedish sections, and for discussions on the topic.

Conflict of interest. None.

References

Albanesi GL and Ortega G (2016) Conodont and graptolite biostratigraphy of the Ordovician System of Argentina. In *Stratigraphy & Timescales* (ed M Montenari), pp. 61–121. Amsterdam: Elsevier.

Bergström SM (1962) Conodonts from the Ludibundus Limestone (Middle Ordovician) of the Tvären area (S.E. Sweden). *Arkiv för Geologi och Mineralogi* **3**, 1–61.

Bergström SM (1964) Remarks on some Ordovician conodont faunas from Wales. Acta Universitatis Lundensis II, 1–67.

Bergström SM (1971) Conodont biostratigraphy of the Middle and Upper Ordovician of Europe and eastern North America. In Symposium on Conodont Biostratigraphy (eds WC Sweet and SM Bergström), pp. 83–157. Boulder: Geological Society of America, Memoir 127.

Bergström SM (1983) Biogeography, evolutionary relationships, and biostratigraphic significance of Ordovician platform conodonts. *Fossils and Strata* **15**, 35–58.

Bergström SM (2007) The Ordovician conodont biostratigraphy of the Siljan region south-central Sweden. A brief review of an international reference standard. In *WOGOGOB 2007. Field Guide and Abstracts* (eds JOR Ebbestad, LM Wickström and AES Högström), pp. 26–41. Uppsala: Sveriges Geologiska Undersöokning (Geological Survey of Sweden) Rapporter och Meddelanden 128.

Bergström SM, Calner M, Lehnert O and Noor A (2011) A new upper Middle Ordovician – Lower Silurian drillcore standard succession from Borenshult in Östergötland, southern Sweden. 1. Stratigraphic review with regional comparisons. *GFF* **133**, 149–71.

Bergström SM, Chen X, Gutiérrez-Marco JC and Dronov A (2009) The new chronostratigraphic classification of the Ordovician System and its relations to major regional series and stages and to δ13C chemostratigraphy. *Lethaia* **42**, 97–107.

Bergström SM and Ferretti A (2017) Conodonts in Ordovician biostratigraphy. *Lethaia* **50**, 424–39.

Bergström SM and Ferretti A (2018) Deciphering the geology of some Darriwilian–Sandbian (Ordovician) 'ghost' formations in the UK and North America using olistoliths in marine debris flows. *Geological Magazine* **155**, 1507–22.

Bergström SM, Finney SC, Chen X, Pålsson C, Wand ZH and Grahn Y (2000) A proposed global boundary stratotype for the base of the Upper Series of the Ordovician system: the Fågelsång section, Scania, southern Sweden. *Episodes* **23**, 102–9.

Bergström SM, Huff WD, Kolata DR and Bauert H (1995) Nomenclature, stratigraphy, chemical fingerprinting, and areal distribution of some Middle Ordovician K-bentonites in Baltoscandia. *GFF* **117**, 1–13.

Bergström SM and Leslie SA (2010) The Ordovician zone index conodont *Amorphognathus ordovicicus* Branson & Mehl, 1933 from its type locality and the evolution of the genus Amorphognathus Branson & Mehl, 1933. *Journal of Micropalaeontology* **29**, 73–80.

Bergström SM and Orchard MJ (1985) Conodonts of the Cambrian and Ordovician systems from the British Isles. In *A Stratigraphical Index of Conodonts* (eds AC Higgns and RL Austin), pp. 32–67. Chichester: Ellis Horwood Limited.

Bergström SM, Rhodes FHT and Lindström M (1987) Conodont biostratigraphy of the Llanvirn-Llandeilo and the Llandeilo-Caradoc Series boundaries in the Ordovician system of Wales and the Welsh Borderland. In *Conodonts: Investigative Techniques and Applications* (ed. RL Austin), pp. 294–315. Chichester: Ellis Horwood Limited.

Bergström SM, Wang Z and Goldman D (2017) Relations between Darriwilian and Sandbian Conodont and Graptolite Biozones. In *Darriwilian to Katian (Ordovician) Graptolites from Northwest China* (eds X Chen, YD Zhang, D Goldman, SM Bergström, JX Fan, ZH Wang, SC Finney, Q Chen and X Ma), pp. 39–78. China: Elsevier & Zhejiang University Press.

Branson EB and Mehl MG (1933) Conodonts from the Maquoketa Thebes (Upper Ordovician) of Missouri. *University of Missouri Studies* **8**, 121–32.

Cocks LRM and Torsvik TH (2005) Baltica from the late Precambrian to mid-Palaeozoic times: the gain and loss of a terrane's identity. *Earth-Science Reviews* **72**, 39–66.

Cooper BJ (1975) Conodonts from the Brassfield Limestone (Silurian) of Southern Ohio. *Journal of Paleontology* **49**, 984–1008.

Dzik J (1976) Remarks on the evolution of Ordovician conodonts. *Acta Palaeontologica Polonica* **21**, 395–455.

Dzik J (1978) Conodont biostratigraphy and paleogeographical relations of the Ordovician Mójcza Limestone (Holy Cross Mts, Poland). *Acta Palaeontologica Polonica* **23**, 51–72.

Dzik J (1990) Conodont evolution in high latitudes of the Ordovician. *Courier Forschungsinstitut Senckenberg* **117**, 1–28.

Dzik J (1994) Conodonts of the Mojcza Limestone. *Acta Palaeontologica Polonica* **53**, 43–128.

Dzik J (1999a) Evolution of the Late Ordovician high-latitude conodonts and dating of Gondwana glaciations. *Bolletino della Società Paleontologica Italiana* **37**, 237–53.

Dzik J (1999b) Relationship between rates of speciation and phyletic evolution: stratophenetic data on pelagic conodont chordates and benthic ostracods. *Geobios* **32**, 205–21.

Feltes NA, Serra F, Ortega G and Albanesi GL (2018) Graptolite and conodont faunas of the Upper Ordovician (Sandbian) successions of the Argentine Precordiellera: biostratigraphic implications. *Geological Journal* **54**, 2301–22.

Ferretti A and Barnes CR (1997) Upper Ordovician conodonts from the Kalkbank limestone of Thuringia, Germany. *Paleontologia* **40**, 15–42.

Ferretti A and Bergström SM (2022) Middle-Upper Ordovician conodonts from the Ffaifach and Golden Grove groups in South Wales, United Kingdom. *Historical Biology* **34**, 462–85.

Ferretti A, Bergström SM and Barnes CR (2014a) Katian (Upper Ordovician) conodonts from Wales. *Palaeontology* **57**, 801–31.

Ferretti A, Bergström SM and Sevastopulo GD (2014b) Katian conodonts from the Portrane Limestone: the first Ordovician conodont fauna described from Ireland. *Bollettino della Società Paleontologica Italiana* **53**, 105–19.

Goldman D, Leslie SA, Nõlvak J and Young S (2007) The Black Knob Ridge section, southeastern Oklahoma, USA: the Global Stratotype-Section and Point (GSSP) for the base of the Katian Stage of the Upper Ordovician Series. *Acta Palaeontologica Sinica* **46**, 144–54.

Goldman D, Sadler PM, Leslie SA, Melchin MJ, Agterberg FP and Gradstein FM (2020) Chapter 20 – the Ordovician Period. In *Geologic Time Scale 2020* (eds FM Gradstein, JG Ogg, MD Schmitz and GM Ogg), pp. 631–694. Amsterdam: Elsevier.

Guenser P, Ginot S, Escarguell G and Goudemand N (2022) When less is more and more is less: the impact of sampling effort on species delineation. *Palaeontology* **65**(3), e12598. doi:10.1111/pala.12598.

Hamar G (1966) The Middle Ordovician of the Oslo Region, Norway. 22. Preliminary report on conodonts from the Oslo-Asker and Ringerike districts. *Norsk Geologisk Tidsskrift* **46**, 27–83.

Harris MT, Sheehan PM, Ainsaar L, Hints L, Männik P, Nõlvak J and Rubel M (2004) Upper Ordovician sequence of Western Estonia. *Palaeogeography, Palaeoclimatology, Palaeoecology* **210**, 135–48.

Hints O, Martma T, Männik P, Nõlvak J, Põldvere A, Shen Y and Viira V (2014) New data on Ordovician stable isotope record and conodont biostratigraphy from the Viki reference drill core, Saaremaa Island, western Estonia. *GFF* **136**, 100–4.

Kaljo D, Martma T and Saadre T (2007) Post-Hunnebergian Ordovician carbon isotope trend in Baltoscandia, its environmental implications and some similarities with that of Nevada. *Palaeogeography, Palaeoclimatology, Palaeoecology* **245**, 138–55.

Leslie SA (2000) Mohawkian (Upper Ordovician) conodonts of eastern North America and Baltoscandia. *Journal of Paleontology* **74**, 1122–47.

Lindström M, Racheboeuf PR and Henry JL (1974) Ordovician conodonts from the Postolonnec Formation (Crozon Peninsula, Massif Armoricain) and their stratigraphic significance. *Geologica et Palaeontologica* **8**, 15–28.

Männik P (2003) Distribution of Ordovician and Silurian conodonts. In *Estonian Geological Sections Bulletin 5, Ruhnu (500) drill core* (ed A Põldvere), pp. 17–23. Tallinn: Geological Survey of Estonia.

Männik P (2004) Recognition of the Mid-Caradoc event in the conodont sequence of Estonia. In WOGOGOB-2004 Conference Materials (eds O Hints and L Ainsaar), pp. 63–64. Tartu: Tartu University Press.

Männik P (2010) Distribution of Ordovician and Silurian conodonts. In *Estonian Geological Sections Bulletin 10, Viki Drill Core* (ed A Põldvere), pp. 21–24. Tallinn: Geological Survey of Estonia.

Männik P (2017) Conodont biostratigraphy of the Oandu Stage (Katian, Upper Ordovician) in NE Estonia. *Estonian Journal of Earth Sciences* **66**, 1–12.

Männik P, Lehnert O, Nõlvak J and Joachimski MM (2021) Climate changes in the pre-Hirnantian Late Ordovician based on δ^{18}O$_{phos}$ studies from Estonia. *Palaeogeography, Palaeoclimatology, Palaeoecology* **569**, 110347. doi: 10.1016/j.palaeo.2021.110347.

Männik P and Viira V (2005) Distribution of Ordovician conodonts. In *Estonian Geological Sections Bulletin 6, Mehikoorma (421) drill core* (ed. A Põldvere), pp. 16–20. Tallinn: Geological Survey of Estonia.

Meidla T, Aainsaar L and Hints O (2014) The Ordovician System in Estonia. In *4th Annual Meeting of IGCP 591, Abstracts and Field Guide*, Estonia, 10–19 June 2014 (eds H Bauer, O Hints, T Meidla and P Männik), pp. 116–22. Tartu: University of Tartu.

Merrill GK (1980) Ordovician conodonts from the Åland Islands, Finland. *GFF* **101**, 329–41.

Nõlvak J, Hints O and Männik P (2006) Ordovician timescale in Estonia: recent developments. Proceedings of the Estonian Academy of Sciences, Geology 55, 95–108.

Nowlan GS (1981) Some Ordovician conodont faunules from the Miramichi Anticlinorium, New Brunswick. *Canadian Government Publishing Centre Supply and Services Canada Bulletin* **345**, 1–35. Ottawa: Geological Survey of Canada.

Orchard MJ (1980) Upper Ordovician conodonts from England and Wales. *Geologica et Palaeontologica* **14**, 9–44.

Ortega G, Albanesi GL, Banchig AL and Peralta GL (2008) High resolution conodont-graptolite biostratigraphy in the Middle-Upper Ordovician of the Serra de La Invernada Formation (Central Precordillera, Argentina). *Geologica Acta* **6**, 161–80.

Paiste T, Männik P and Meidla T (2022) Sandbian (Late Ordovician) conodonts in Estonia: distribution and biostratigraphy. *GFF* **144**, 9–23.

Paiste T, Männik P, Nõlvak J and Meidla T (2020) The lower boundary of the Haljala Regional Stage (Sandbian, Upper Ordovician) in Estonia. Estonian Journal of Earth Sciences 69, 76–90.

Põldvere A (ed.) (2005) *Estonian Geological Sections Bulletin 6, Mehikoorma (421) drill core*. Tallinn: Geological Survey of Estonia, 67 pp.

Purnell MA, Donoghue PCJ and Aldridge RJ (2000) Orientation and anatomical notation in conodonts. *Journal of Paleontology* **74**, 113–22.

Pyle LJ and Barnes CR (2002) *Taxonomy, Evolution, and Biostratigraphy of Conodonts from the Kechika Formation, Skoki Formation, and Road River Group (Upper Cambrian to Lower Silurian), Northeastern British Columbia*. Ottawa: NRC Research Press, 227 pp.

Rhodes FHT (1953) Some British Lower Palaeozoic conodont faunas. *Philosophical Transactions of the Royal Society of London, Series B* **237**, 261–334.

Saadre T, Einasto R, Nõlvak J and Stouge S (2004) Ordovician stratigraphy of the Kovel-1 well (Volkhov-Haljala) in the Volynia region, northwestern Ukraine. *Bulletin of the Geological Society of Denmark* **51**, 47–69.

Savage NM and Bassett MG (1985) Caradoc-Ashgill conodont faunas from Wales and the Welsh Borderland. *Palaeontology* **28**, 679–713.

Serra F, Albanesi GL, Ortega G and Bergström SM (2015) Biostratigraphy and palaeoecology of Middle–Late Ordovician conodont and graptolite faunas of the Las Chacritas River section, Precordillera of San Juan, Argentina. *Geological Magazine* **152**, 813–29.

Stouge S (1998) Distribution of conodonts in the Tartu (453) core, Appendix 12. In *Estonian Geological Sections Bulletin 1, Tartu (453) drill core* (ed. P Männik). Tallinn: Geological Survey of Estonia.

Stouge S, Bauert G, Bauert H, Nõlvak J and Rasmussen JA (2016) Upper Middle to lower Upper Ordovician chitinozoans and conodonts from the Bliudziai-150 core, southern Lithuania. *Canadian Journal of Earth Sciences* **53**, 781–7.

Sweet WC (1981) Macromorphology of elements and apparatuses. In *Treatise on Invertebrate Paleontology* (ed RA Robinson), Pt. W, Miscellanea, Supplement 2, Conodonta, W5–W20. Lawrence: Geological Society of America and University of Kansas Press.

Sweet WC (1988) *The Conodonta: Morphology, Taxonomy, Paleoecology, and Evolutionary History of a Long-extinct Animal Phylum*. Oxford: Clarendon Press, 212 pp.

Sweet WC, Ethington RL and Barnes CR (1971) North American Middle and Upper Ordovician conodont faunas. In Symposium on Conodont Biostratigraphy (eds WC Sweet and SM Bergström), pp. 163–93. Colorado, Boulder: Geological Society of America, Memoir 127.

Sweet WC and Schönlaub HP (1975) Conodonts of the genus Oulodus Branson & Mehl, 1933. *Geologica et Palaeontologica* **9**, 41–59.

Viira V (1974) Ordovician Conodonts of the East Baltic. Tallinn: Valgus, 143 pp. (in Russian with English summary).

Viira V (2008) Conodont biostratigraphy in the Middle-Upper Ordovician boundary beds of Estonia. *Estonian Journal of Earth Sciences* **57**, 23–38.

Viira V, Aldridge RJ and Curtis S (2006) Conodonts of the Kiviõli Member, Viivikonna Formation (Upper Ordovician) in the Kohtla section, Estonia. Proceedings of the Estonian Academy of Sciences, Geology 55, 213–40.

Webby BD, Cooper RA, Bergström SM and Paris F (2004) Stratigraphic framework and time slices. In *The Great Ordovician Biodiversification Event* (eds BD Webby, F Paris, ML Droser and IG Percival), pp. 41–7. New York: Columbia University Press.

Xu C, Bergström SM, Yuandong Z, Goldman D and Qing C (2010) Upper Ordovician (Sandbian–Katian) graptolite and conodont zonation in the Yangtze region, China. *Earth and Environmental Science Transactions of the Royal Society of Edinburgh* **101**, 111–134.